PET/MRI in Brain Tumors

11

Ida Sonni, Valentina Garibotto, Andrei Iagaru, Devsmita Das, and Tarik Massoud

Contents

11.1 Introduction

The poor clinical outcome of intracranial malignancies makes them a major medical problem. According to the American Cancer Society, 23,700 new cases of primary brain tumors would be diagnosed in the United States in 2016 [1]. Brain metastases

I. Sonni (✉)
Department of Radiology, Nuclear Medicine and Molecular Imaging, Stanford University, Stanford, CA 94305, USA
e-mail: isonni@stanford.edu, idasonni@gmail.com

V. Garibotto
Division of Nuclear Medicine and Molecular Imaging, Geneva University Hospitals, Geneva, Switzerland

NIMTlab, Faculty of Medicine, Geneva University Hospitals, Geneva, Switzerland

A. Iagaru • D. Das • T. Massoud
Department of Radiology, Division of Neuroimaging and Neurointervention, Stanford University, Stanford, CA 94305, USA
e-mail: aiagaru@stanford.edu

A. Iagaru et al. (eds.), *PET/MRI in Oncology*,
https://doi.org/10.1007/978-3-319-68517-5_11

are more common than primary brain tumors as 10–20% of adults with cancer develop metastases to the brain. Even though any malignancy could potentially metastasize to the brain, in the majority of cases, they arise from lung, breast, and skin (melanoma) cancers [2]. Primary brain tumors are a heterogeneous group of neoplasms including different subtypes with a wide range of histopathologic, molecular, and genetic profiles and consequently different clinical presentation and prognosis. The complex pathophysiology and vast heterogeneity of brain tumors make their classification confusing to the most, despite the World Health Organization (WHO) provides us with detailed classification. The fourth edition of the *WHO Classification of Tumors of the Central Nervous System* (CNS) published in 2007 [3] describes numerous tumor entities, variants of entities, and histological patterns. As a means of predicting the biological behavior of the tumor, histological grading is also described. Brain tumors are divided in four grades, primarily based on aggressiveness (Table 11.1). An update of the fourth *WHO Classification of Tumors of the Central Nervous System* was recently released in 2016 [4] and represents a conceptual and practical advance to the 2007 version. In the molecular era that we are living, when a better insight into tumor biology and tumor genetic profiles is warranted, the last updated WHO classification incorporated molecular parameters, in addition to histology, in the definition of many tumor entities [4, 5]. The role played by neuroimaging in this complex scenario is essential. Particularly important is the use of molecular imaging and new advanced magnetic resonance imaging (MRI) techniques that can aid tumor characterization noninvasively, allowing a more targeted therapeutic approach, and consequently improve prognosis of these tumors.

One of the several aspects that make brain tumors unique compared to other systemic tumors is the presence of the blood-brain barrier (BBB) [6]. Brain blood vessels are protected by this selective barrier limiting the exchange of substances between the systemic and cerebral circulations. This aspect is extremely important because the BBB, besides protecting the brain from external insults, may also limit the permeability to contrast media (e.g., gadolinium), to some radiopharmaceuticals for SPECT or PET imaging, as well as some therapeutic agents. The most aggressive brain tumors (high grades), due to their infiltrative growth pattern, are accompanied by disruption of the BBB. But when tumor growth is slow and does not affect BBB integrity (low grades), this may represent a challenge to tumor visualization [6, 7]. Another issue related to the unicity of the BBB is the so-called

Table 11.1 Brain tumor grading

Grading	Proliferative activity	Clinical behavior
Grade I (well differentiated)	Low proliferative potential	Usually curable by surgical resection
Grade II (moderately differentiated)	Low proliferative potential	Recurrence is frequent
	Infiltrative	Tend to progress to higher grades
Grade III (poorly differentiated)	Brisk mitotic activity and nuclear atypia	Tend to recur often
	Infiltrative	
Grade IV (undifferentiated)	Mitotically active	Rapid pre- and postoperative evolution
	Necrosis-prone	Fatal outcome

pseudoprogression [8]. In patients with malignant gliomas treated with radiation therapy, it was found an increase in contrast-enhanced lesions on MRI immediately after treatment that improved without any further treatment. This condition has been defined pseudoprogression, to be distinguished from actual tumor progression, and is due to treatment-induced temporary loss of integrity of the BBB allowing gadolinium enhancement [9].

These important aspects should be considered when imaging brain tumors with contrast-enhanced MRI and PET/CT or PET/MRI.

MRI with and without contrast is the mainstay imaging modality for diagnosis, treatment planning, and posttreatment response assessment of brain tumors [10, 11]. Structural MRI provides excellent anatomical detail, and more advanced recently implemented techniques allow evaluation of metabolic or functional information regarding brain tumors. Molecular imaging with PET can also play an important role in brain tumors, especially in those gray areas where usefulness of MRI is limited.

This chapter will review the main features of different MR techniques and PET radiopharmaceuticals used in brain tumors imaging. The current applications of integrated PET/MRI systems will be described in the final sections, as well as the advantages of the combined approach.

11.2 Neuroimaging of Brain Tumors

11.2.1 Computed Tomography (CT)

In patients with suspected brain tumors, CT remains the first-line imaging modality. This is mainly due to its widespread availability, ease of the procedure, low costs, and relatively low risks, and it is usually well tolerated by patients. CT is very sensitive in identifying mass effect, acute hemorrhage, hydrocephalus, and other structural alterations due to the presence of brain tumors. However, the poor soft tissue contrast of CT represents a major drawback in imaging the brain and limits its ability to detect the subtle changes in brain parenchyma that accompany brain tumors in some cases. Other worth-mentioning disadvantages of CT are the radiation exposure due to the use of ionizing radiations and the high allergenic potential of iodinated contrast agents. For all the reasons described above, CT remains an initial screening technique in patients with suspected brain tumors, but its utility is limited to the exclusion of life-threatening conditions [6, 12].

11.2.2 Magnetic Resonance Imaging (MRI)

Magnetic resonance imaging (MRI) has become a critically important and obligatory diagnostic tool central to the multidisciplinary planning and clinical management of brain tumor patients [13–16]. The inherent high resolution and exquisite soft tissue contrast of MRI allow to gain an understanding of the three-dimensional morphologic and functional features of brain tumors and thus to appreciate the problem these neoplasms pose in patient clinical management. These imaging strategies also allow the fusion of disparate sets of information regarding brain tumors

(e.g., structural, functional, hemodynamic, metabolic, and cellular) into the clinical assessment of patients. Neuroimaging-based MRI tools may therefore be used to diagnose brain tumors and suggest their aggressiveness preoperatively, to plan and guide surgical biopsy or removal intraoperatively, to understand any potential complications arising from treatment, and to assess and monitor therapeutic response and patient prognosis.

Current clinical management of patients with brain tumors depends entirely on the use of up-to-date neuro-MRI techniques. Recent advances in brain tumors imaging offer unique anatomical and pathophysiological information that provide new insights into brain tumor biology and behavior. Here we discuss both structural and advanced MRI methods for the diagnosis of brain tumors, their treatment planning, and for disease monitoring, highlighting the modern clinical application of these techniques in evaluation and treatment of brain tumor patients. A detailed consideration of the underlying MR physics is beyond the scope of this chapter and can be found elsewhere in this book. Instead, we discuss the modern clinical application of neuro-MRI in the daily evaluation and treatment of patients with brain tumors.

11.2.2.1 Structural MRI of Brain Tumors

There are several reasons why structural MRI has a central role in the neuroradiologic assessment of brain tumors [5, 17]. First, because of its relative advantages over CT imaging, it is usually the first study that allows an accurate diagnosis of a brain tumor. Not only can small tumors be missed on CT scanning but this technique may not depict all multifocal lesions. Detailed morphological characteristics as well as the presence of leptomeningeal or intraventricular spread may also be difficult to diagnose on CT scanning. Second, accurate structural characterization, both qualitative and quantitative, of a brain tumor, as reflected in its pathological MRI signal, is crucial for defining the topographical features of the tumor and, in turn, its likely natural history if left untreated. Third, the analysis of these structural MRI features is crucial in helping select the most appropriate treatment. Finally, MRI is used after tumor resection for assessing the extent of tissue removal—the extent of resection, along with histopathology, being two important factors in determining patient prognosis. There are two recent areas of research and development aimed at enhancing the contributions of structural MRI to brain tumor management. One approach uses methods that allow more accurate image segmentation especially of the peripheral zones of tumor infiltration into surrounding cerebral parenchyma to enable better assessment of tumor margins, and the other is the adoption of VASARI (Visually Accessible Rembrandt Images) feature set criteria to provide a more objective standard and use of a numerical score to quantitatively describe the nature and extent of tumor MRI features.

Different chemical compositions and molecular environments in the brain lead to different MRI relaxation times. Both T1 and T2 relaxation times vary for different tissue types and depend on field strengths. T1-weighted images (T1WIs) are best for obtaining contrast between different healthy brain tissues. However, most pathology, including brain tumors, has long T2 and long T1 (high signal on T2WIs and low signal on T1WIs). Structural MRI is generally concerned with visualizing soft

tissue, e.g., brain or tumor parenchyma, or properties derived from the structural integrity of these tissues. Thus, different tumor components have different T1 and T2 values, depending on tissue composition, e.g., tumor, necrosis, edema, hemorrhage, and calcification. In practice, multi-sequence MRI is therefore used to better characterize brain tumors, especially those with aggressive features. The standard protocol most commonly used includes spin-echo T2-weighted images (T2WIs) (Fig. 11.1a), fluid-attenuated inversion recovery images (FLAIR) (Fig. 11.1b), T1-weighted images (T1WIs) (Fig. 11.1c), T1WI after the administration of contrast agent (Fig. 11.1d), and gradient echo images (GRE) (Fig. 11.1e) [18–20]. Most tumors are hypointense on T1WIs and hyperintense on T2WIs in the absence of hemorrhagic changes. In biologically aggressive tumors such as glioblastoma, MRI usually shows a heterogeneous mass with internal cysts, flow voids representing prominent intratumoral vessels, internal T1 hyperintense areas (hemorrhagic foci), neovascularity, necrotic foci, significant peritumoral vasogenic edema, infiltration of surrounding brain, and significant mass effect on adjacent normal brain structures that become effaced or distorted. The structural imaging features of commonly encountered brain tumors are described in Table 11.2. Because of the highly variable appearance of brain tumors, they may mimic other brain diseases on MRI. For example, a glioblastoma cystic mass with rim enhancement may be mistaken for other brain tumors, tumefactive demyelination, radiation necrosis, metastasis, subacute abscess, an infarct, or a resolving hematoma. A low-grade glioma may be mistaken for an infarct, demyelination, cerebritis, or hamartoma. In terms of the imaging appearance of a mass in the spectrum from low-grade glioma to glioblastoma, the following generalizations can be made, although with exceptions: the incidence of calcification decreases toward glioblastoma, whereas the incidence increases toward glioblastoma for enhancement, hemorrhage, necrosis, mass effect, and surrounding vasogenic edema.

The use of gadolinium chelate contrast-enhanced imaging of the brain has become a standard and essential part of the evaluation of most brain pathologies. The accurate delineation of areas with blood-brain barrier (BBB) disruption depends on the contrast sensitivity of the applied MRI technique and the dosage and type of gadolinium-based contrast agent. The latter has been extensively studied for the diagnosis of various diseases including detection of primary or secondary brain tumors where the use of single- or multiple-dose applications of gadolinium contrast agents has been proven.

Fluid-attenuated inversion recovery (FLAIR) imaging is an MRI sequence achieved by applying an inversion pulse with a long recovery time between this pulse and the start of the measurement. It may be used to suppress the high CSF signal on T2WIs so that the pathology adjacent to CSF spaces may be seen more clearly. Also, subtle lesions in the cortex stand out against of the background of attenuated CSF. Vasogenic edema surrounding brain tumors is also better seen and defined on FLAIR images and is therefore used in conjunction with T2WIs. Contrast-enhanced FLAIR MRI may be used by taking advantage of the T1 effect to achieve a particularly high contrast between tumor and background tissue. This allows an exact separation of enhancing and nonenhancing tumor components on

one sequence. Two- and three-dimensional FLAIR techniques are simple to implement. Three-dimensional Cube FLAIR also has the advantage of increased number of image slices that can be reconstructed in three planes.

In the pulse sequence of gradient echo (GRE) MRI, the repetition time (TR) can be reduced because flip angles other than 90° are used. This results in shorter imaging times and less motion artifacts. Therefore, GRE MR images are very sensitive to flow,

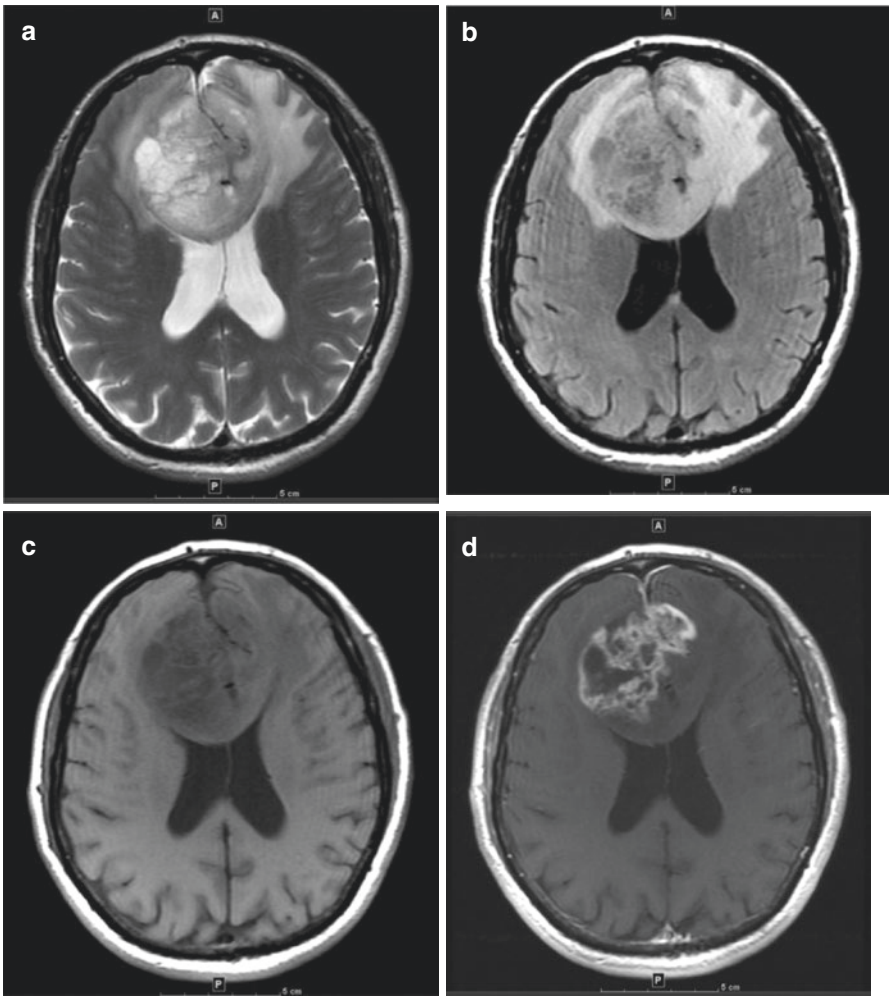

Fig. 11.1 Selected axial MR images of a 78-year-old patient with a large glioblastoma in bilateral anterior frontal lobes and spreading across the anterior corpus callosum (butterfly lesion). (**a**) T2WI shows the multicystic tumor and mass effect on the lateral ventricles. (**b**) Better delineation of the surrounding vasogenic edema on FLAIR T2WI. (**c**) T1WI. (**d**) Irregular heterogeneous thick nodular enhancement on a post-contrast T1WI. (**e**) Patchy increased susceptibility effect (signal dropout) on GRE, suggesting minimal intratumoral hemorrhage. (**f**, **g**) Patchy tumor restricted diffusion on DWI (**f**) and confirmed as dark signal on the ADC map (**g**). (**h**) Increased cerebral blood flow in the anterior aspects of this tumor seen on bolus perfusion imaging

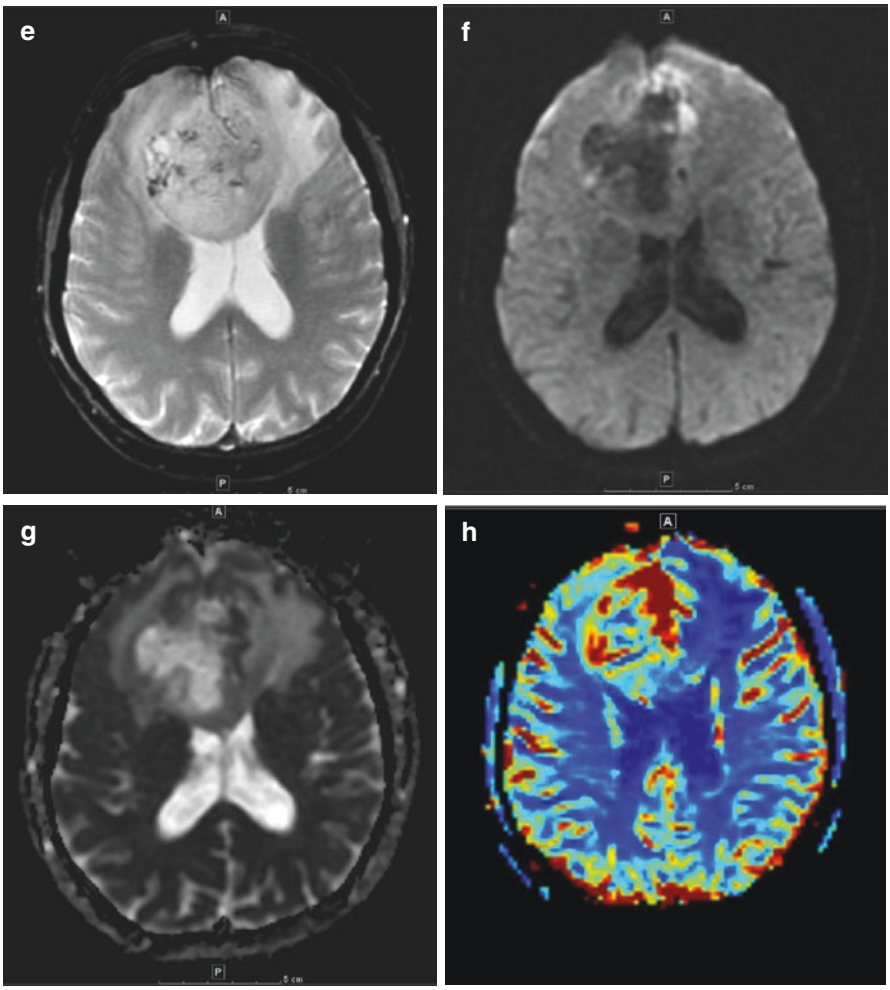

Fig. 11.1 (continued)

can produce images that produce MR angiographic sequences, and also may be used to see regions of signal dropout within a mass that represent calcification or slow flow within tumor vessels. Calcified tumors produce areas of signal void, and GRE pulse sequences are also very sensitive to the presence of hemorrhage, showing signal void owing to increased susceptibility effects. GRE is especially suited to three-dimensional imaging, which is used when high-resolution and thin contiguous slices are required, e.g., in performing time-of-flight MR angiography.

11.2.2.2 Advanced and Functional MRI of Brain Tumors

Over the past three decades, we have witnessed a shift in neuro-oncologic imaging from merely providing structural and anatomical information toward providing additional information about tumor physiology [21, 22]. Newer advanced MRI

Table 11.2 MRI features of selected common glial and other brain tumors

Tumor	T1 features	T2 features	Others
Glioblastoma	Isointense to hypointense	Hyperintense with surrounding edema	Variable enhancement that is peripheral, irregular, nodular. Necrosis. Hemorrhagic products. Variable restricted diffusion. On MRS: choline, lactate, lipids: increased; NAA, myoinositol: decreased
Diffuse astrocytoma (low-grade glioma)	Isointense to hypointense	Mass-like hyperintense. Follows white matter but expands the cortex	No restriction or enhancement. On MRS choline, choline: creatine ratio, and myoinositol and mI/Cr ratio: increase; NAA: decreased. No lactate peak
Pilocytic astrocytoma	Isointense to hypointense	Hyperintense solid component	Usually large cystic component with a brightly enhancing mural nodule. Enhancement. May have calcification
Pleomorphic xanthoastrocytoma	Isointense to hypointense	Isointense to hyperintense	Mural nodule. May have dural tail and remodeling of adjacent skull
Meningioma	Isointense to hypointense	Isointense to hypointense	Extra-axial. Intense enhancement. May show restricted diffusion. CSF vascular cleft sign. Dural tail. Sunburst appearance of vessels. May have vasogenic edema
Metastases	Isointense to hypointense. If hemorrhagic or melanoma, then may be hyperintense	Hyperintense	Uniform, punctate, or ring enhancement. Peritumoral edema may be out of proportion to tumor size
Vestibular Schwannoma	Isointense to hypointense	Heterogeneously hyperintense	Strong contrast enhancement, heterogeneous in large tumors

Table 11.2 (continued)

Tumor	T1 features	T2 features	Others
Ependymoma	Isointense to hypointense	Hyperintense	Foci of blooming from hemorrhage or calcification on GRE. Necrosis, but may be solid. Heterogeneous enhancement. Restricted diffusion
Medulloblastoma	Hypointense	Isointense to hyperintense	Most enhance. Calcification, necrosis, cysts. Surrounding edema. Restricted diffusion Usually vermian, but in adults is more lateral cerebellar
Oligodendroglioma	Hypointense	Hyperintense except for calcification areas	May enhance and show variable increased perfusion

techniques for brain tumors include diffusion and diffusion tensor imaging with tractography, perfusion imaging, MR spectroscopy, and functional imaging using the blood oxygenation level-dependent (BOLD) technique. These MRI techniques allow obtaining a variety of multiparametric information regarding brain tumor pathophysiology and investigating the structural, functional, and metabolic nature of brain tumor microenvironment. The evolution of these techniques has come about from a need for clinical researchers and pharmaceutical companies to have access to early and noninvasive biological information regarding brain tumors that can predict outcome and/or quantify therapeutic efficacy. Therefore, the readouts from these advanced MRI strategies are currently being used clinically, and further investigated as biomarkers for early diagnosis, for predicting outcome in response to specific therapies and monitoring therapeutic efficacy.

Diffusion-Weighted Imaging (DWI)

Diffusion-weighted imaging (DWI) is a unique tissue contrast technique based on a pulse sequence sensitized to the random motion of water molecules, i.e., Brownian motion. Certain pathologies constrain the normal Brownian motion of water molecules in brain tissue (restricted diffusion). Lesions that have restricted diffusion appear hyperintense on DWI and hypointense on the accompanying apparent diffusion coefficient (ADC) maps. Factors such as tissue perfusion, transport of water, or bulk motion can also contribute to the signal loss on ADC; this being the reason why the term ADC is used instead of diffusion coefficient. Thus, it is possible to quantify the diffusion in brain tissues by analyzing the accompanying ADC map. Differences in ADC arise owing to intracellular and extracellular diffusion, cellularity, cell membrane permeability, and overall tissue structure.

In brain tumors, DWI can be helpful in preoperative radiological grading of gliomas [23, 24]. Restricted diffusion in peripheral solid components of a glioma is attributed to hypercellularity and high nuclear to cytoplasmic ratios (Fig. 11.1f, g), corresponding to higher tumor grades, which include anaplastic astrocytoma and glioblastoma, whereas low-grade astrocytomas display increased diffusivity. Other brain tumors that typically show restricted diffusion for similar reasons are lymphoma, medulloblastoma, and meningioma (except that calcified or psammomatous meningiomas have low ADC values). Furthermore, epidermoid cysts almost always display restricted diffusion. DWI can also be used to discriminate tumor tissue from edema or a cystic or necrotic portion of a tumor. The latter may appear hypointense on DWI and show much higher ADC values, whereas the areas of enhancing tissue on T1WIs show high signal intensity on DWI. DWI is also very useful for differentiating a brain abscess from necrotic or cystic tumor. Abscesses have high central restriction on DWI owing to the presence of pus (in the center of a ring enhancing lesion) that restricts water motion within its cavity. An acute arterial infarct will also show bright restricted diffusion on DWI owing to cytotoxic edema.

Diffusion Tensor Imaging and Tractography

Diffusion tensor imaging (DTI) is an imaging technique to study the microarchitecture of brain parenchyma by quantifying physical parameters such as fractional anisotropy (FA) and mean diffusivity [25]. It is centered on the concepts of isotropic and anisotropic diffusion. Since water molecules can diffuse equally in all three directions, this is termed isotropic diffusion. This is found in the cerebral ventricles, but also occurs in gray matter. Instead, free water molecules move anisotropically in white matter, i.e., diffusion of water is not equal in all three directions. In white matter tracts, the myelin sheaths surrounding nerves cause the water molecules to move along the long axis of a fiber bundle and less in other directions. Thus, maximum diffusivity coincides with the orientation of white matter fiber tracts. Consequently, DTI allows identification and characterization of white matter tracts according to the direction and degree of their anisotropic water diffusion.

Information from DTI can be presented in two formats, FA maps and tractography (Fig. 11.2). Quantification of FA can provide an indication of white matter development and degradation. FA maps are images obtained in cross section. These may be formatted in gray scale or may be color coded to depict information on direction of white matter tracts. Conventionally, commissural white matter tracts, e.g., the corpus callosum, are shown in red, association fibers such as the superior longitudinal fasciculus are shown in green, and the superior-inferior running projection fibers are seen in blue. The intensity of color hues is proportional to the extent of FA. It is possible also to generate three-dimensional representations of the major white matter tracts in the brain. The principle direction of diffusion in a voxel is called the eigenvector. Tractography is performed by connecting a given voxel to the appropriate adjacent voxel, in accordance with the orientation of each voxel's principal eigenvector.

One of the most important indications of DTI in clinical practice is to study the relation of a brain tumor to white matter tracts [26]. Within a tumor center white

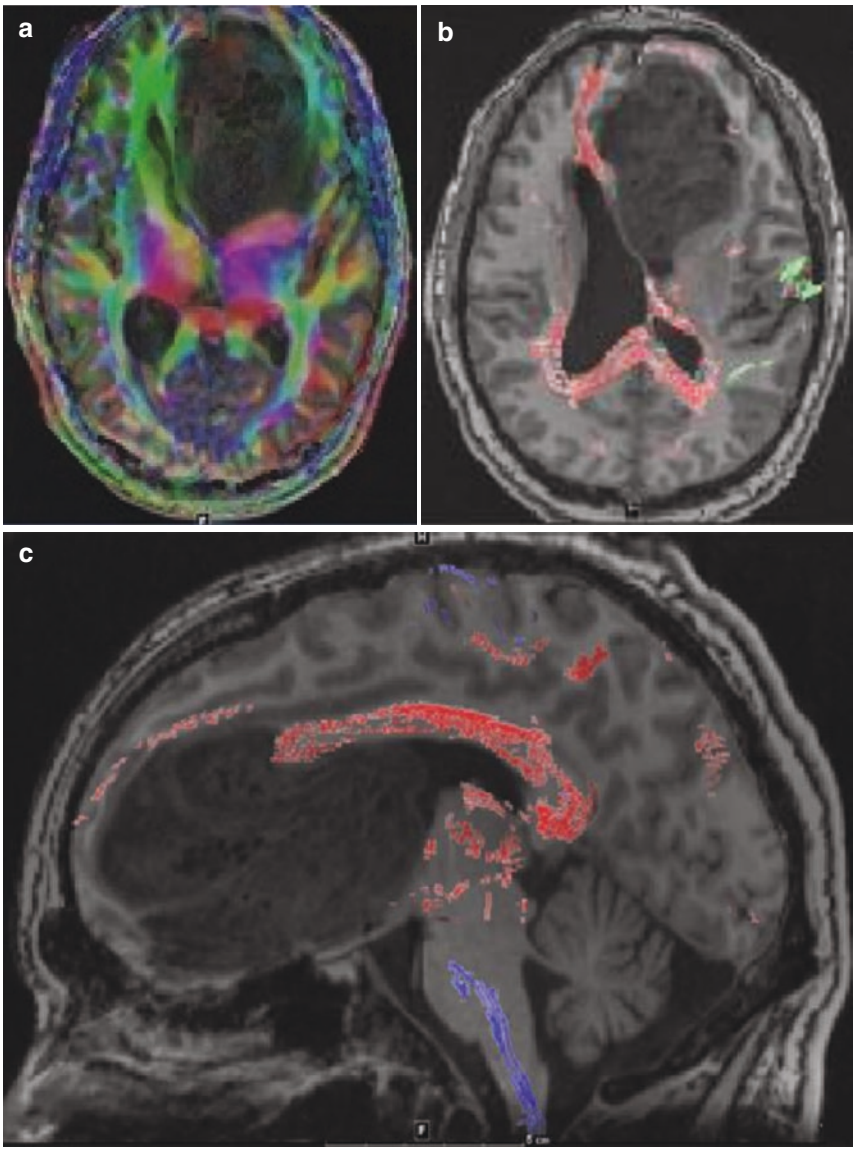

Fig. 11.2 Selected MR images of a 26-year-old patient with a large glioblastoma in the anterior left frontal lobe. (**a**) Axial DTI. (**b**) Axial tractography. (**c**) Sagittal tractography

matter fibers are displaced by cellular infiltration and FA is reduced. A tumor can displace, invade, and destroy surrounding white matter tracts or cause vasogenic edematous changes within them. Therefore, in the periphery and in a narrow rim of white matter rim surrounding a tumor, FA may be preserved or even increased by fiber compression owing to the mass effect of the tumor. When a white matter tract

is destroyed by tumor, there is loss of FA and therefore a reduction in their values, manifested on the gray scale FA maps as a loss of brightness.

There may be FA changes in white matter indicating cellular infiltration beyond the area of tumor enhancement. This can help guide the surgical approach and extent of resection. DTI demonstration of the corticospinal tracts may be used in conjunction with intraoperative fiber stimulation. Preoperative tractography demonstrating tumor involvement of the corticospinal tracts has been correlated to motor deficits, even without involvement of the motor cortex. Normalization depicted on postoperative tractography can predict improvement in function, suggesting a useful prognostic role for intraoperative tractography.

Bolus Perfusion Imaging

Perfusion-weighted imaging provides information about the perfusion status of the cerebral microcirculation [27]. There are two main approaches to measure cerebral perfusion using MRI. The first is application of an exogenous intravascular contrast agent, usually gadolinium-based, to highlight either the susceptibility effects of the contrast agent on the signal echo, namely, first-pass dynamic susceptibility contrast-enhanced (DSC) MR perfusion, or the relaxivity effects of the contrast agent on the signal echo, namely, dynamic contrast-enhanced (DCE) MR perfusion. The second approach is to capitalize on the presence of an endogenous contrast agent by using magnetically labeled arterial blood water as a diffusible flow tracer in arterial spin labeling (ASL) MR perfusion, discussed below. In DSC MR perfusion (or bolus-tracking MRI), the first pass of a bolus of contrast agent through the brain is monitored by a series of T2- or T2*-weighted MR images. The susceptibility effect of the paramagnetic contrast agent results in a signal loss, demonstrated on the signal intensity-time curve. Using the principles of the indicator dilution theory, the signal information can then be converted into a contrast medium concentration-time curve on a pixel-by-pixel basis. From these data, parametric maps of cerebral blood volume (CBV) and flow (CBF) can be derived. Regional CBF and CBV values can be obtained by region-of-interest analysis. DCE is based on the acquisition of serial T1WIs before, during, and after administration of a gadolinium-based contrast agent. The resulting signal intensity-time curve reflects a composite of tissue perfusion, vessel permeability, and extravascular-extracellular space. Using pharmacokinetic modeling of perfusion data, several metrics are commonly derived, of which the most frequently used is k^{trans} and which appears to reproducibly measure permeability in glioma patients.

Perfusion imaging using MRI has become an integral component of the complete radiological assessment of brain tumors [28]. Tumor-associated neoangiogenesis produces very high blood volume in tumor tissue. Thus, the increased capillary density in the tumor causes markedly elevated CBV and CBF (Fig. 11.1h), as compared to normal brain parenchyma. Perfusion imaging is often useful to establish the diagnosis of tumor and to distinguish tumor from tumor mimics, such as abscess or tumefactive demyelination, which show hypoperfusion with low values of CBV and CBF.

Perfusion imaging can noninvasively help evaluate tumor grade. Low-grade astrocytomas are hypoperfused as compared to high-grade lesions. Up to one-third

of the high-grade tumors do not enhance, which may lead to a false radiological impression of low grade. Thus, a perfusion study can demonstrate hyperperfusion associated with higher grade. Moreover, since primary high-grade tumors are infiltrative by nature, their peritumoral edema show elevated CBV values. By contrast, metastases are well marginated and noninfiltrative by nature, and their perilesional edema is purely vasogenic with low CBV values.

CBV maps may also be used to delineate tumor margins. The results of stereotactic biopsy on high-grade tumors such as glioblastomas are frequently negative, and this may be because the tissue sampling has not been obtained from the most aggressive part of the lesion. MR perfusion may therefore help direct the localization of stereotactic biopsies from the most aggressive components of morphologically heterogeneous tumors. Perfusion can also differentiate tumor recurrence from enhancing nonneoplastic tissue such as radiation necrosis (causing an endarteritis) which would also be useful for surgical planning and targeting of biopsies and radiation therapy. Perfusion imaging will likely be increasingly used as a surrogate marker to study response to newer antiangiogenic pharmaceuticals in clinical trials.

Arterial Spin-Labeling Perfusion Imaging

Arterial spin labeling (ASL) is a newer perfusion technique that does not require exogenous contrast, and instead it exploits the spins of endogenous water protons that perfuse the imaging plane. It thus uses electromagnetically labeled arterial blood water as a freely diffusible intrinsic tracer. In clinical applications, this technique has proved reliable and reproducible in the assessment of CBF in various pathologic states, including cerebrovascular and neurodegenerative diseases, and temporal lobe epilepsy [29]. There is also a general positive correlation between ASL signal intensity and density of microvessels in brain tumors. ASL may be useful in differentiating between high- and low-grade gliomas; distinguishing glioblastomas from metastases, CNS lymphomas, and all other glioma grades; and predicting the outcome for metastatic brain tumors after radiosurgery [30]. Hemangioblastomas have significantly higher ASL signal than gliomas, meningiomas, and schwannomas.

Magnetic Resonance Spectroscopy

MRS is a noninvasive technique capable of measuring chemicals within the body. MRS distinguishes various metabolites based on their slightly different chemical shifts or resonance frequencies. Nuclei that can be analyzed using MR are those possessing odd numbers of protons and neutrons, e.g., ^{1}H, ^{31}P, ^{13}C, ^{19}F, and ^{23}Na. Of these, the most commonly used is hydrogen or proton spectroscopy. The metabolic information received is displayed as a graph, with the resonance frequencies plotted on the x-axis to identify each unique metabolite. These frequencies (in parts per million, ppm) are plotted on the y-axis. MRS can analyze single or multiple voxels of the brain. Multivoxel MRS is also called chemical shift imaging (CSI). When using CSI it is possible to construct color maps of metabolites that spatially demonstrate their peaks and ratios. These maps are overlapped with conventional MR images to demonstrate anatomical localization.

Clinically relevant metabolites that feature on a brain spectral graph are branch-chained amino acids, lipid, lactate, alanine, N-acetyl aspartate (NAA), choline, creatine, and myoinositol. MRS can help in establishing the diagnosis of tumor by demonstration of elevated choline, a metabolite that is found in normal brain but is raised in tumors owing to high cell turnover. Indeed, the characteristic spectral graph of a glioma depicts depressed NAA (a neuronal marker), elevated choline and lipid, and/or lactate peaks [21, 31, 32]. It is thus possible to differentiate tumors from other lesions such as abscesses or radiation necrosis. Moreover, when elevated choline is found in peritumoral edema, it may suggest a diagnosis of primary glioma rather than metastasis. Meningiomas, on the other hand, are characterized by elevated alanine. The disadvantages of MRS are that it has poor spatial resolution and it is sometimes nonspecific.

Hyperpolarized ^{13}C MRS

The emergence of hyperpolarized ^{13}C MRS has opened many new possibilities for novel metabolic imaging studies that are translatable to the clinic and can serve to characterize brain tumors and their response to therapy [32, 33]. ^{13}C MRS studies have been challenging owing to the significantly low intrinsic sensitivity of the technique, and when using ^{13}C-labeled compounds, long acquisition times are required, currently limiting the application of this method in patient studies.

Molecules containing NMR-visible nuclei, such as ^{13}C, can be hyperpolarized using dissolution dynamic nuclear polarization. This allows hyperpolarization and dissolution of ^{13}C-labeled compounds that cause an increase in their signal-to-noise ratio by 10,000–50,000-fold as compared with thermal equilibrium. To achieve this, the labeled compound, mixed with a free radical, is placed at low temperature (<2 K) and at high magnetic field (3–5 T). Microwave irradiation then saturates the electron spin resonance, and polarization is transferred from the radical electron to the labeled nucleus. This leads to an increase in polarization from parts per million to 10–50%. However, a limitation of hyperpolarized agents is their lifetime. Relaxation times are typically less than a minute. A meaningful brain study therefore requires rapid dissolution and injection of the hyperpolarized agents, as well as rapid transport across the BBB and a fast metabolic rate. In addition, a rapid data acquisition strategy is required. This has led to a trade-off between spatial resolution and acquisition time. In spite of these challenges, several hyperpolarized ^{13}C agents as well as novel imaging methods have been developed over the past decade to specifically image metabolic pathways that are reprogrammed in brain tumors. This new imaging approach enables study of major metabolic pathways and their reprogramming in cancer in real-time, noninvasively, and with no ionizing radiation involved.

Functional MRI

Functional MRI (fMRI) demonstrates brain function with neuroanatomic localization on a real-time basis. Cortical activity may be studied by fMRI techniques based on detecting focal blood flow and oxygenation changes following neuronal activity,

using BOLD contrast, which requires the detection of very small signal intensity changes, 0–3% at 1.5 T and up to 6% at 3 T, for voxel volumes as small as 3 × 3 × 5 mm. In the BOLD technique, the performance of a predefined cognitive task leads to regionally increased neuronal activity and consequent localized hemodynamic changes that produce a measurable signal. Thus, neural activation is followed by an increase in local blood flow and an increase of oxygenated hemoglobin in the capillaries of the activated brain tissue. The parallel drop in concentration of paramagnetic deoxyhemoglobin leads to a focal signal increase in the affected tissue using T2* sequences (the BOLD effect). This was first used to demonstrate activated brain regions as a result of sensory or motor stimulation.

BOLD imaging in the brain has many useful applications, e.g., localizing neuronal activities, display of areas affected by sensory stimuli or motor activation, and as a noninvasive tool for presurgical mapping of cortical function in patients with intracranial tumors [34, 35]. fMRI imaging is primarily used to preoperatively establish the relationship of a brain tumor to eloquent cortex. The latter may show significant anatomical variability and displacement by the mass effect from a tumor. Although functional MR imaging cannot yet replace intraoperative electrocortical stimulation in patients undergoing neurosurgical tumor resection, it may be useful in guiding surgical planning and mapping, thereby reducing the extent and duration of craniotomy. Thus, fMRI can contribute to more efficient surgical removal of both benign and malignant brain tumors with an increase in patient survival and a decrease in surgical morbidity. In addition, it is necessary to establish hemispheric dominance for language processing preoperatively in brain tumor patients. A preoperative fMR imaging study of language processing provides information on the feasibility of surgical resection and allows adequate assessment of the risk of neurological deficits in the postoperative period. Unfortunately, fMRI is currently unable to distinguish critical areas for brain function, whose resection would lead to permanent disability, from accessory or modulatory brain areas that may be resected without significant postoperative disability.

11.2.2.3 Radiogenomics of Gliomas

Genomic characterization has recently improved the assessment of glioblastoma by describing distinct molecular gene expression profiles, underlying genomic abnormalities, and epigenetic modifications. Radiogenomic mapping (a link between MRI features and underlying molecular data) can potentially address the clinical need for surrogate imaging biomarkers that accurately predict underlying tumor biology and therapy response in glioblastoma [36–39]. For this, gene expression modules are first constructed from information on glioblastomas, e.g., those available in The Cancer Genome Atlas (TCGA), depicting extensive molecular characterization, including gene expression, copy number, and DNA methylation status for each tumor. By correlating quantitative image features with such modules, we can hypothesize on how gene expression patterns may drive the morphologic manifestations captured by quantitative MRI features. The VASARI MRI feature set is a system designed to enable consistent description of gliomas using a

set of defined visual features and controlled vocabulary. These standardized VASARI feature-set criteria are 30 qualitative and quantitative imaging features that describe the size, location, as well as numerous detailed morphological characteristics of a tumor. MRI features of a tumor have been shown to noninvasively reflect to some extent its biology and pathology, tumor microenvironment, and its genomic makeup.

11.2.2.4 Challenges in MRI of Glioblastoma

There are some limitations and challenges to MRI assessment when defining glioblastoma progression and treatment response [17, 40, 41]. First, glioblastomas are frequently irregular in shape and may change anisotropically or differentially in response to therapy, which limits meaningful linear tumor measurements. In addition, visible contrast-enhancing components are not necessarily representative of active tumor volume. The Response Assessment in Neuro-Oncology (RANO) Working Group has suggested criteria for response assessment that include evaluation of nonenhancing areas of tumor. Further, nonenhancing active tumor components and therapy-related changes in enhancement are well-recognized challenges. Radiation necrosis may manifest as edema and a range of nonspecific enhancement patterns, which can be impossible to distinguish from true progression or recurrence of tumor using MRI.

Radiological pseudoprogression, where transient increases in apparent tumor size and enhancement are seen during and shortly after aggressive chemoradiation, is increasingly recognized. Thus, within 12 weeks of chemoradiation, progression should only be considered on imaging if there are areas of new enhancement outside the field of radiation treatment. Pseudoprogression is more common in tumors with favorable methylation status of methylated O6-methyl guanine-DNA methyltransferase (MGMT), and these tumors show better overall treatment response.

Steroid treatment has been shown to decrease BBB permeability and regional CBV (pseudoresponse). Controlling for steroid treatment is therefore important when imaging patient response. Similarly, antiangiogenic agents specifically targeted to vascular endothelial growth factor are used to treat glioblastoma, and may have a complex effect upon vasculature, which in turn modulates contrast enhancement. Accordingly, appearances on MRI following antiangiogenic treatment may mask residual or recurrent disease by showing decreased enhancement without actual tumor regression. Therefore, contrast enhancement alone is not a suitable marker for tumor response in this context.

11.2.3 Positron Emission Tomography (PET)

PET imaging of brain tumors is increasingly used in clinical practice. PET is typically a second-level investigation in patients already evaluated by MRI or in conjunction with it when hybrid technology is available.

The interest of PET imaging is thus to complement MRI for specific questions that are only partially addressed by MRI, namely: (1) contribute to the diagnostic

Table 11.3 Current potential indications of the main PET radiopharmaceuticals used in brain tumors imaging

PET radiopharmaceutical	Diagnosis	Grading	Therapy-induced changes vs. recurrence	Therapy monitoring	Tumor extent delineation
^{18}F-FET, ^{11}C-MET	✓	✓	✓	✓	✓
^{18}F-FDOPA	–	–	✓	✓	✓
^{18}F-FDG	–	–	✓	✓	✓
^{18}F-FMISO	–	✓	–	✓	–
^{18}F-FPPRGD$_2$	–	–	–	✓	–
^{18}F-FLT	✓[a]	✓	✓[a]	✓[a]	✓[a]
^{11}C-Acetate	–	✓	–	–	–
^{18}F- and ^{11}C-Choline	✓	✓	✓	–	✓
^{68}Ga-DOTA-peptides	✓[b]	✓[b]	✓[b]	✓[b]	✓[b]

[a]In high-grade gliomas
[b]In meningiomas

process of intracranial masses of unknown origin, (2) help grading lesions to establish the appropriate management and target the highest grade component for biopsy planning, (3) define tumor extent for surgical and radiation therapy planning, (4) evaluate treatment response, and (5) differentiate between treatment-induced changes and disease recurrence (Table 11.3).

This section will describe the most important PET radiopharmaceuticals used in brain tumors imaging with a description of their advantages and drawbacks, as well as a brief review of the literature on currently available studies conducted using PET/CT.

11.2.3.1 Radiolabeled Amino Acids (^{11}C-MET) and Amino Acid Analogues (^{18}F-FET, ^{18}F-DOPA)

Brain tumors are characterized by a higher protein metabolism than normal brain tissue and inflammatory lesions; therefore, protein synthesis can represent a good diagnostic marker. L-type amino acid transporter1 (LAT1) is a membrane protein responsible for amino acid (AA) transport through the cell membrane and is typically overexpressed in glial tumors, as well as in case of blood-brain barrier (BBB) rupture, which can modulate and increase AA delivery. AA analogue radiopharmaceuticals have low uptake in normal brain tissue, whereas tumor lesions present as focal uptake on PET imaging.

The first radiopharmaceutical of this extensively used class is ^{11}C-methionine (MET), an essential sulfur AA necessary for cellular proliferation and growth [42]. MET is not only transported within the cells by LAT1 but is also incorporated into proteins, even if its uptake is correlated with methionine transport and not directly with protein synthesis [43]. Its use is mainly limited by the short half-life of ^{11}C, which confines its application to hospitals equipped with an onsite cyclotron. ^{18}F-Fluoro-ethyltyrosin (FET) has been more recently developed and has gained larger use, since fluorinated tracers can be easily delivered in multiple sites [44]. Its

distribution and binding properties are similar to those of MET, with the characteristic of a slower clearance, associated with a higher blood pool signal that might hamper the analysis of regions close to the venous sinuses [45]. Comparative studies have shown similar diagnostic properties and a strong correlation of quantitative measures such as tumor-to-background ratio (TBR) of MET and FET [46].

^{18}F-DOPA is another AA analogue, sharing the same mechanism of uptake by LAT1 as MET and FET. It has been shown that the uptake and distribution of DOPA and MET are overall comparable [47].

A comparative study including DOPA and FET has highlighted some differences, namely, a faster kinetic both in high- and low-grade gliomas and a high contrast to background in extrastriatal regions for DOPA [48]. Indeed, DOPA might have a higher sensitivity in low-grade tumors, as compared with the performances reported for other AA analogues [49]. Its physiologic uptake in the basal ganglia represents the main limitation for use in lesions close to the basal ganglia, even if this can be partly overcome by scanning rapidly after injection (20 min) to limit specific binding to dopamine receptors [47]. In addition, it does not show higher uptake in oligodendroglial lesions, as reported for other AA analogues (see below).

Finally, preliminary data report the use in brain tumors of a synthetic AA analogue, ^{18}F-FACBC, or fluciclovine, a tracer mainly tested in prostate cancer [50, 51].

The use of AA analogues has been examined for all previously mentioned applications. Recently, recommendations for clinical use of PET imaging have been published by the Response Assessment in Neuro-Oncology (RANO) Working Group [52].

Lesion Characterization/Diagnosis

The sensitivity of MET for identification of tumoral lesions is in the range of 80%, with some low-grade lesions having lower uptake, while specificity is higher, around 90% [53, 54].

A meta-analysis has shown that FET PET has a pooled sensitivity of 82% and pooled specificity of 76% to differentiate primary brain tumors from non-tumoral intracranial lesions and suggested a TBRmean of 1.6 and TBRmax of 2.1 as cutoff values [55].

For lesion characterization, almost all high-grade gliomas, brain metastases, and oligodendrogliomas have intense uptake, while false negative (10–30%) might occur in low-grade tumors [53]. Non-tumoral lesions have usually less or no uptake, even if high FET uptake has been reported in hematoma, radiation necrosis, ischemic stroke, and abscesses, given the passive tracer influx in case of rupture of the BBB [56].

Grading and Biopsy Planning

The uptake value on static imaging does not provide reliable grading information with any AA tracer, even if higher-grade tumors usually show higher uptake in case of high-grade tumors [57]. Furthermore, a higher uptake in oligodendroglial, 1p19q codeleted tumors has been reported both for FET and for MET [54, 58, 59]. The significant overlap between grades and the association with histological type does not allow a reliable tumor assessment at an individual level, but justifies the interest of targeting a high uptake region, if any, for biopsy planning, and previous studies

have shown its usefulness [60, 61]. The uptake can also have prognostic value, differentiating benign and grade I lesions from higher-grade lesions for MET [62, 63], for FET [64], and for DOPA [65].

The analysis of the evolution over time of tracer uptake in FET PET dynamic scans provides additional information on tumor grading [66]. Lower-grade lesions or non-tumoral lesions typically show an increasing uptake over time and a late time to peak, more than 15/20 min (pattern I), while higher-grade tumors are typically characterized by an early uptake (less than 15/20 min) followed either by a plateau (pattern II) or a washout (pattern III) [58]. The added value of this analysis has been shown in grading lesions and in characterizing recurrent lesions vs. radiation necrosis [67]. A similar behavior, namely, an early peak in higher-grade lesions, has been reported for DOPA images [68, 69], while it has not been observed for MET [70].

Tumor Delineation and Radiation Therapy Planning

The tumor delineation based on molecular information is able to capture the infiltrative component without BBB rupture and the low-grade component, both for surgical and radiation therapy planning.

The comparative accuracy of AA PET imaging for radiation therapy planning has been compared in a review, showing that both MET and FET have good performances, variable across series but in the range of 90% [71]. A good performance has also been reported in a series of patients evaluated by DOPA [72]. A threshold of 1.6 with contralateral physiological uptake has been suggested for lesion segmentation on the basis of a biopsy-controlled study [73]. Multiple studies concordantly show that the volumes determined on the basis of PET and MRI differ significantly [74]. [75]–[79].

A tumor delineation using the molecular information has shown a positive prognostic impact in a small population study, not confirmed in a subsequent larger study [80, 81]. A randomized controlled trial is ongoing to test the added value of PET in radiation therapy planning [82].

The presence of a residual uptake has negative prognostic value, while the presence of residual contrast enhancement had not [60, 83].

Therapy Response Monitoring

A few studies have shown that AA PET typically shows low uptake in cases of pseudoprogression [46, 84]. AA PET imaging might also identify progressive disease under bevacizumab treatment earlier than MRI, with a favorable impact on costs [85, 86].

The majority of these studies used FET, showing that, after temozolomide, a reduction of TBRmax higher than 20% has a positive prognostic value [87] and that, after bevacizumab, a reduction of more than 45% of the metabolically active volume has a positive prognostic value [88].

The added value in surgical planning has been shown for MET and for DOPA [72, 89, 90].

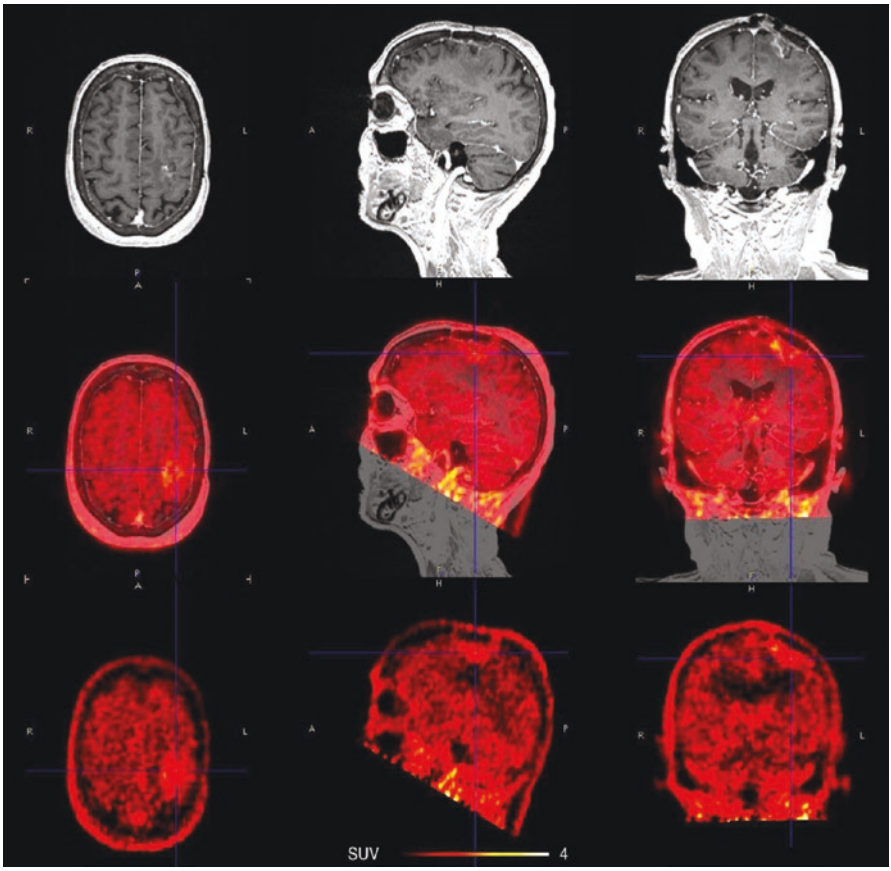

Fig. 11.3 ^{18}F-FET PET/MRI images showing a moderate uptake (SUVmean 1.5) increasing over time (pattern III) in a histologically proven radiation necrosis. From left to right, axial, sagittal, and coronal view. From top to bottom, MRI, fused PET/MRI images, and FET PET images

Differential Diagnosis Recurrence/Treatment-Induced Changes

MET, FET, and DOPA PET have been tested for differentiating high-grade tumor/metastasis recurrence and treatment-induced changes, reporting high sensitivity and more variable, but overall high specificity, providing additional information as compared to MRI (Fig. 11.3) [66, 67, 91–94].

11.2.3.2 Glucose Metabolism (^{18}F-FDG)

^{18}F-FDG is the most commonly used radiopharmaceutical in oncology, given the strong association between cellular proliferation and glucose metabolism in most tumors. Importantly, ^{18}F-FDG PET uptake is not influenced by BBB rupture, increasing its specificity. However, its use in the brain is limited by the physiologic uptake of the normal brain cortex, which uses glucose as the main metabolic substrate. This limitation can be partly overcome using later imaging times, over 5 h

after administration [95, 96]. A second limitation is the potent effect of corticosteroids, often used to treat edema associated with intracranial masses, on brain tumors' ^{18}F-FDG uptake, through the increase of glycemia and the reduction of cerebral blood volume [97].

The use of ^{18}F-FDG for differential diagnosis of intracranial masses is a well-established indication in differentiating toxoplasmosis and primary lymphoma, reaching a sensitivity and specificity higher than 90%; toxoplasmosis lesions show ^{18}F-FDG uptake lower than the gray matter uptake (SUVmax in the range of 2–6), while lymphomas have uptake higher than the gray matter (SUVmax in the range from 12 to 30) [98].

For grading and prognostic evaluation, ^{18}F-FDG imaging can be useful in glial tumors: low-grade tumors (WHO grades I and II) have an activity in the range of normal white matter, WHO grade III tumor uptake is close to the gray matter activity, and WHO grade IV tumors might have focally higher uptake, with inhomogeneities related to tumor necrosis [99]. A higher tumor-to-normal brain ratio has been consistently associated with shorter survival [100]. For this reason different diagnostic cutoffs with the white matter and cortical activity have been suggested for low- and high-grade glioma, with good sensitivity and specificity [101, 102]. There are relevant exceptions represented by histological types with high glucose metabolism despite a low grade, such as gangliolioma and pilocytic astrocytomas [103]. Non-glial tumors, namely, lymphomas, also have a high ^{18}F-FDG uptake [104]. ^{18}F-FDG cannot be used for tumor delineation, because of negative findings in low-grade tumors/components and because of the high physiologic metabolism of the brain.

For treatment monitoring, a change in management in 38% of patients was observed in a large series of either primary brain tumors or metastases based on the National Oncologic PET Registry [105].

For differentiating tumor recurrence and treatment-related changes, ^{18}F-FDG PET reaches a good sensitivity of 96% but variable specificity [106] [107]. One study directly compared the performance of MET and ^{18}F-FDG for this indication, showing a higher sensitivity and interrater agreement of MET [63].

11.2.3.3 Tumor Hypoxia (^{18}F-MISO) and Angiogenesis (^{18}F-FPPRGD$_2$)

Tumor Hypoxia The concept that radiosensitivity of tumor cells is increased in the presence of oxygen has been long known [108]; consequently, it has been thought that tumor hypoxia may have a major importance in the efficacy of radiation therapy, with hypoxic tissues being more radioresistant. Decades of research have brought us to the conclusion that tumor hypoxia changes gene expression patterns in tumor cells, leading to more aggressive survival traits and altering their malignant potential [109, 110]. Tumor hypoxia plays a crucial role in tumor cell survival, tumor development, and resistance to treatment, therefore, it is an attractive target for PET radiopharmaceuticals development [111]. The noninvasive assessment of tumor hypoxia by means of PET could help select patients, prior to radiation therapy treatments that may benefit from the use of radiosensitizing drugs. The

most extensively investigated PET radiopharmaceutical for tumor hypoxia imaging is ^{18}F-fluoromisonidazole (^{18}F-MISO), which showed a good potential in identifying hypoxic brain tumors. It accumulates in tissues binding to intracellular macromolecules when pO_2 is very low ($pO_2 < 10$ mmHg) [109] and in the periphery of the tumor, but not in the necrotic center, because only viable, hypoxic tissue can accumulate the radiopharmaceutical [112]. ^{18}F-MISO has been used in several clinical trials [113, 114], with the first study in humans published in 1992 by Valk et al. [115]. In this proof-of-concept study, three patients affected by malignant gliomas were evaluated, and feasibility of ^{18}F-MISO PET, as well as its ability to detect tumor hypoxia, was demonstrated. 15 years later, in a larger cohort of 22 patients with glioblastoma multiforme, Spence et al. have demonstrated that the hypoxic burden, measured using ^{18}F-MISO PET, impacts time to tumor progression and overall survival in patients previously treated with surgical intervention [116]. Some groups evaluated the possible role of ^{18}F-MISO PET in differentiating tumor grade [117, 118] with promising results, but larger cohorts might be needed to confirm clinical utility. Other groups investigated a possible correlation between tumor hypoxia, measured with ^{18}F-MISO PET, and glucose metabolism, measured with ^{18}F-FDG PET, suggesting discordance between the two modalities [119, 120], but the combination of the two studies was seen to be predictive of progression-free survival and overall survival in glioblastoma patients [121]. Similar results were seen for ^{18}F-MISO PET and MRI in a recently published multicenter study involving 42 patients with glioblastoma and aimed at assessing tumor hypoxia with the two imaging modalities. The lack of strong correlation between PET and MRI parameters shows their complementary role in the assessment of tumor status. Overall, the parameters measured by MRI (tumor blood volume/flow, vascular permeability) and hypoxia measured by ^{18}F-MISO PET are strongly correlated to prognosis in newly diagnosed glioblastoma patients [122].

Angiogenesis There is considerable evidence that hypoxia is strictly connected to angiogenesis, another key player in tumor growth and metastatization [123, 124]. More aggressive and malignant brain tumors have shown an abundant vascular proliferation histologically, and the vascular microenvironment highly influences the pathophysiological characteristics of the tumor [124]. Since angiogenesis has emerged in the last decade as a major target for drug development for malignant brain tumors, it also spurred interest toward the development of PET radiopharmaceuticals that may guide antiangiogenic treatment [125–127]. ^{18}F-FPPRGD$_2$ is a PET radiopharmaceutical targeting integrin $\alpha_v\beta_3$, which is highly expressed in proliferating vascular endothelial cells and plays an important role in angiogenesis [128]. Iagaru et al. used ^{18}F-FPPRGD$_2$ in the evaluation of 17 patients affected by glioblastoma multiforme and suspected recurrence. Patients were imaged before and after treatment with bevacizumab, and PET measured parameters, i.e., SUV_{max} and angiogenesis volume, were shown to be correlated to prognosis.

Despite the high potential utility of hypoxia and angiogenesis PET radiopharmaceuticals, too little is yet available on large cohorts of patients, therefore the use of these families of radiopharmaceuticals is still limited to research settings.

11.2.3.4 Other Radiopharmaceuticals (Radiolabeled Choline, ^{11}C-acetate, ^{18}F-FLT, Somatostatin Receptor)

Phospholipid Synthesis Choline is an essential substrate for biosynthesis of phosphatidylcholine, a major component of all cell membranes. Cancer cells have an increased cellular metabolism compared to normal cells, which entails an increased need of choline, and therefore an increased uptake of radiolabeled choline detected by PET [113]. Choline can be radiolabeled with either ^{11}C or ^{18}F. ^{11}C-Choline and natural choline are biochemically indistinguishable, whereas ^{18}F-labeled choline, ^{18}F-fluoroethyl-choline (FEC), and ^{18}F-fluoromethyl-choline (FCH) have shown some differences in pharmacokinetics that were not however observed in clinical settings [129, 130]. Radiolabeled choline has been used in a variety of tumors, but the main application remains prostate cancer. In brain tumors radiolabeled choline has been used for the first time in 1997, when Hara et al. described very encouraging results in visualization of brain tumors in 24 patients using ^{11}C-choline. High ^{11}C-choline uptake was seen in brain tumors, as opposed to very low uptake in the surrounding healthy brain parenchyma, allowing easy tumor delineation [131]. Different groups have found that radiolabeled choline is able to differentiate high-grade gliomas (high choline uptake) from low-grade gliomas (low choline uptake) [132, 133], whereas another group found contrasting results [134]. Choline was found able to differentiate benign from malignant lesions [135, 136] and also brain metastases (highest choline uptake) from high-grade gliomas (higher uptake than benign lesions, but lower than brain metastases) and benign lesions (low choline uptake) [137]. In a cohort of 94 patients with suspected brain tumors, Huang et al. found that ^{11}C-choline, despite a superior diagnostic accuracy in comparison to ^{18}F-FDG, had a rate of false positive of 4.55% and false negative of 3.64% [138]. When compared to ^{11}C-methionine, radiolabeled choline had a worse performance than the amino acid analogue in terms of visual evaluation of tumor localization [139] and also in the differential diagnosis between brain tumors and monofocal acute inflammatory demyelination (MAID), a demyelinating disease associated with MRI characteristics (e.g., gadolinium enhancement, edema, and mass effect) mimicking brain malignancies [140]. In the differential diagnosis between tumor recurrence and radionecrosis, radiolabeled choline performed better than MRI and ^{18}F-FDG [141]. In a posttreatment scenario, radiolabeled choline showed good diagnostic accuracy in the detection of recurrence of high-grade glioma [142] and in low-grade gliomas with equivocal findings on other imaging during follow-up [143]. ^{11}C-Choline uptake was also described in patients affected by meningiomas [144]. Despite some studies showing excellent results using radiolabeled choline in brain tumors, the role of the radiopharmaceutical has not been clearly defined yet.

Tumor Proliferation The increase of cell proliferation rate is a key characteristic of cancer; consequently, the identification of an accurate imaging biomarker of cell

proliferation in vivo would be highly desirable. Thymidine, the only nucleoside exclusively incorporated in DNA and not in RNA, has been evaluated for this purpose. It has been initially radiolabeled with ^{11}C [145], but due to the short half-life of the radioisotope (20 min) and the rapid in vivo degradation of ^{11}C-thymidine, it was considered less suitable for clinical use [146]. The thymidine analogue 3-deoxy-3′-[^{18}F]-fluorothymidine (^{18}F-FLT), developed by Shields et al. in 1998, has more favorable characteristics and is now the most widely used PET radiopharmaceutical for imaging and measuring tumor proliferation. ^{18}F-FLT is taken up and phosphorylated by the enzyme thymidine kinase-1 (TK-1), whose activity is strongly related to cell proliferation, and then trapped in the cell [113, 146]. A recent kinetic analysis study showed that ^{18}F-FLT uptake is more significantly correlated to BBB disruption than to TK-1 phosphorylation activity [147]. The high dependency of ^{18}F-FLT uptake from BBB damage is well known and represents a major disadvantage when evaluating low-grade gliomas, since they are usually not associated with BBB damage. In a comparative evaluation of ^{18}F-FDOPA, ^{18}F-FDG, and ^{18}F-FLT in 15 patients with low-grade gliomas, Tripathi et al. conclude that ^{18}F-FLT PET should not be used in the evaluation of recurrent low-grade gliomas because of its limited utility [148]. Several groups demonstrated that ^{18}F-FLT PET can be useful in grading gliomas and particularly in identifying high-grade gliomas and differentiating them from low grades [149–154]. ^{18}F-FLT has been directly compared to ^{18}F-FDG showing a much better tumor-to-background contrast and better tumor visualization due to the high glucose metabolism and negligible ^{18}F-FLT uptake in normal brain tissue. In a recent meta-analysis, Li et al. showed that ^{18}F-FLT has a better overall diagnostic accuracy in the detection of recurrent gliomas than ^{18}F-FDG [155]. In comparison with the amino acid analogue ^{11}C-MET, ^{18}F-FLT showed a lower sensitivity for tumor detection, but better correlation to cell proliferation index Ki-67, and better tumor grading assessment in gliomas of different grades [154, 156]. In the differential diagnosis between tumor recurrence and radionecrosis, ^{18}F-FLT has been compared to ^{18}F-FDG and ^{11}C-MET in two studies, and both showed no clear superiority of one radiopharmaceutical over the other [157, 158]. The most important application of ^{18}F-FLT seems to be therapy monitoring in high-grade gliomas. Different groups showed that ^{18}F-FLT is a good predictor of progression-free survival and overall survival in patients treated with the antiangiogenic drug bevacizumab [159–163]. ^{18}F-FLT was also used in a large Phase II trial evaluating newly diagnosed glioblastoma patients treated with everolimus, temozolomide, and radiation therapy [164].

Acetate Acetate is a metabolic substrate of β-oxidation and precursor of cholesterol and amino acids. In the cell, it is activated to acetyl-CoA via the enzyme acetyl-CoA synthase, which can follow two different metabolic pathways, depending on the cell type. In myocardial cells, it is mainly oxidized in the mitochondria by the tricarboxylic acid (TCA) cycle, whereas in tumor cells, it is mainly converted into fatty acids which are incorporated into phosphatidylcholine, an important component of cell membranes [165]. Due to its potential role in imaging myocardial cells and tumor proliferating cells, acetate has been radiolabeled with ^{11}C for PET

imaging and initially used for imaging of myocardial oxidative metabolism [166]. In oncology, ^{11}C-acetate is primarily used in prostate cancer imaging, but it has also been evaluated in brain tumors. Different groups showed that ^{11}C-acetate can be useful in grading of brain tumors (gliomas, astrocytomas, and meningiomas), allowing a clear differentiation between high grade and low grade [167–170]. In a comparative study with ^{18}F-FDG and ^{11}C-MET for the evaluation of gliomas, Yamamoto et al. found that ^{11}C-acetate has a better sensitivity than ^{18}F-FDG, but lower than ^{11}C-MET [170].

Somatostatin Receptors Somatostatin receptors (SSTR) are G-protein-coupled membrane glycoproteins that have received, particularly during the last two decades, large interest due to their overexpression in neuroendocrine tumors (NETs). Five subtypes of human SSTR have been identified so far (SSTR-1–SSTR-5) with different expressions and functions. Various PET radiopharmaceuticals targeting SSTRs have been developed, with variable binding affinities to the different SSTR subtypes. The most used are DOTA-TOC, DOTA-TATE, and DOTA-NOC, radiolabeled with ^{68}Ga using the universal chelator DOTA, which forms stable complexes in vivo [171]. Due to the high expression of SSTRs in meningiomas, mostly SSTR-2 [172], several studies have investigated ^{68}Ga-DOTA-peptides in imaging meningiomas. In 2001, Henze et al. described their first experience using ^{68}Ga-DOTA-TOC in a small cohort of patients with meningiomas, finding very promising results and excellent imaging properties of the PET radiopharmaceutical, including very high target-to-background ratio. Several groups described the utility of PET imaging using ^{68}Ga-DOTA-peptides in tumor extent delineation, particularly in the setting of therapy planning [173–179]. ^{68}Ga-DOTA-TATE has been described by Sommerauer et al. as a reliable predictor of tumor growth in WHO I and II meningiomas [180]. In a large study involving 134 patients comparing ^{68}Ga-DOTA-TOC PET to contrast-enhanced MRI in the detection of meningiomas, PET showed a better sensitivity than MRI (190 lesions identified by PET vs. 171 by contrast-enhanced MRI), confirming the importance of the imaging modality also in the diagnostic setting [181]. Another attractive application of PET using ^{68}Ga-DOTA-peptides is the possibility of theranostics, due to the radiolabeling of DOTA-peptides with β^-emitting radioisotopes for peptide receptor radionuclide therapy (PRRT) [182]. Some groups have evaluated ^{68}Ga-DOTA-peptides in the setting of PRRT for meningiomas, showing that ^{68}Ga-DOTA-peptides PET allows pre-therapeutic assessment of tumor radionuclide uptake in PRRT [183] and can be predictive of outcome [184].

11.3 Integrated PET/MRI in Brain Tumors Imaging

The introduction of integrated PET/CT tomographs in the clinical practice has represented a milestone opening a new era for hybrid imaging. The added value of the simultaneous acquisition of PET and CT goes far beyond the sum of the utilities deriving from the two single modalities performed separately. The thought that the success obtained with PET/CT could be replicated with PET/MRI was obvious.

Table 11.4 PET/MRI studies in brain tumors imaging

Reference	Patient population	Radiopharmaceutical/ MR sequences	Aim	Conclusions
[189]	7 healthy volunteers	^{11}C-MET/standard diagnostic MRI, DTI	Feasibility of DTI using simultaneous PET/MRI	DTI is feasible using the combined approach without degradation of image quality
	4 patients with BT			
[191]	4 patients with BT	^{18}F-FET /standard diagnostic MRI, DTI, MRS, fMRI	Feasibility of simultaneous PET/MR	Description of acquisition protocols
[190]	15 patients (in total)	^{18}F-FET/standard diagnostic MRI, PWI, DTI	Test performance and clinical applicability of combined approach	Combined approach is feasible in a clinical setting
	5 patients with BT:			Satisfactory results
	2 GBM			
	1 low grade			
	1 grade IV			
	1 choroid plexus carcinoma			
[188]	28 patients with BT	^{11}C-MET/standard diagnostic MRI, MRS	Feasibility of simultaneous approach for grading purposes using metabolic mapping	Metabolic mapping of gliomas before histological sampling is feasible using the combined approach
	16 low grade			
	12 high grade			
[197]	10 patients with BT:	^{11}C-MET and ^{68}Ga-DOTA-TOC/ standard diagnostic MRI	Comparison with PET/CT	Combined approach can be reliably performed in BT imaging. Image quality and quantification are similar to PET/CT
	3 low grade		Feasibility and accuracy of combined approach	
	1 grade III			
	2 GBM			
	2 atypical neurocytoma			
	3 meningioma			
[198]	50 patients in total	^{18}F-FDG, ^{11}C-MET, and ^{68}Ga-DOTA-TOC/ standard diagnostic MRI, DTI, ASL, and proton spectroscopy	Comparison with PET/CT	Quality of MRI images using the combined PET/MRI approach is uncompromised. Results are in high accordance with PET/CT
	29 patients with BT		Image quality of PET/MRI	

(continued)

Table 11.4 (continued)

Reference	Patient population	Radiopharmaceutical/ MR sequences	Aim	Conclusions
[192]	15 patients with meningioma (33 lesions identified)	^{68}Ga-DOTA-TOC/ standard diagnostic MRI	Comparison with PET/ CT. Feasibility of the combined approach	PET/MRI provides flawless image quality
[193]	26 patients with BT (post-surgery and chemo-RT)	^{18}F-FET/standard diagnostic MRI, DWI, perfusion EPI, MRS	Differentiation of therapy-induced changes from recurrence in glioma patients	FET uptake with Cho/Cr ratio and normalized rCBVmean can distinguish glioma recurrence from radiation necrosis
[194]	20 patients with BT	^{18}F-FDG/standard diagnostic MRI, PWI	Differentiation of therapy-induced changes from recurrence. Tumor grading	PWI has better diagnostic accuracy in differentiating therapy-induced changes from recurrence than PET
[196]	4 pediatric patients: 2 grade I 1 grade III 1 GBM	^{11}C-MET/standard diagnostic MRI	Evaluation of ^{11}C-MET PET/ MRI in preoperative biopsy planning and navigation in pediatric patients	PET/MRI provides high-resolution data for neuronavigation reducing radiation exposure and avoiding additional anesthesia in very young patients
[195]	12 pediatric patients with astrocytic tumors: 8 low grade 4 high grade	^{18}F-Choline/standard diagnostic MRI	Feasibility of the combined approach for diagnosis and response assessment	^{18}F-Choline PET/ MRI is a reliable imaging tool. It permits therapy monitoring
[199]	69 patients with high-grade gliomas	^{11}C-MET/standard diagnostic MRI	Role of ^{11}C-MET PET/MRI in tumor volume evaluation for RT planning	The use of PET/ MRI did not change the target volumes defined on FLAIR MRI
[200]	56 patients with gliomas	^{18}F-FET/standard diagnostic MRI, PWI	Direct comparison of ^{18}F-FET to PWI using PET/MRI	^{18}F-FET PET and PWI yield different information

BT brain tumors, *GBM* glioblastoma multiforme, *DTI* diffusion tensor imaging, *MRS* MR spectroscopy, *fMRI* functional MRI, *ASL* arterial spin labeling, *PWI* perfusion-weighted imaging

One of the settings where a combination of PET and MRI could be more useful is undoubtedly the study of the brain, where a high soft tissue delineation and high resolution are particularly relevant. After the initial attempt to simultaneously acquire PET and MR data in 1997 [185], the first study conducted in humans was a brain study by Schlemmer et al., published one decade later [186]. Fully integrated PET/MRI scanners for humans are available for whole-body imaging since the end of 2010 [187], and their valuable role in research settings is unquestionable. But the real clinical utility of integrated PET/MRI still needs to be proven and sustained by large prospective trials. The focus of this section will be on the current applications of integrated PET/MRI systems, specific advantages of a combined PET/MRI approach in neuro-oncology, and future perspectives.

11.3.1 Current Applications of PET/MRI in Brain Tumors

Only limited literature is currently available and is summarized in Table 11.4. The initial studies conducted using integrated PET/MRI scanners were aiming at assessing feasibility of the combined approach and confirmed that it is feasible and does not degrade image quality of the single modalities [186, 188–191]. Some groups evaluated performances of PET/MRI in comparison to the well-established hybrid PET/CT in the evaluation of brain tumors. Afshar-Oromieh et al. [192] studied 15 patients affected by meningiomas with ^{68}Ga-DOTA-TOC PET/MRI in comparison to PET/CT. Image quality of PET/MRI was described as flawless, but the authors state that the small dimension of their cohort doesn't allow a meaningful comparison, and this would require larger studies. In another study, comparing the performance of PET/CT and PET/MRI in the same population of ten patients affected by different brain tumors, Boss et al. describe similar image quality and quantification. PET/MRI has also been used in the setting of differential diagnosis between therapy-induced changes (radionecrosis and pseudoprogression) and tumor recurrence. Contrast-enhanced MRI cannot distinguish the two conditions, and different PET radiopharmaceuticals have been found superior to MRI for this purpose [52]. Two different groups have evaluated combined PET/MRI in this setting with promising results [193, 194]. Another clinical setting where PET/MRI has been successfully evaluated is that of pediatric patients with brain tumors. In such populations, the reduction of iodizing radiation exposure and number of examinations (with better patient comfort and reduced sedation time in very young patients) deriving from PET/MRI may play a crucial role in the success of the combined approach [195, 196].

11.3.2 Specific Advantages of the Simultaneous PET/MRI Approach in Neuro-oncology

The individual characteristics of PET and MRI in the evaluation of brain tumors have been described in detail above. As for PET/CT, the advantages of the combined PET/MRI approach are greater than the sum of its parts. Before the introduction of

simultaneous PET/MRI scanners, research has been focusing on developing software for co-registration of the two separate examinations, but this approach can be affected by substantial differences in image quality. The simultaneous acquisition of PET and MRI in hybrid scanners allows an optimal temporal and spatial co-registration in one single imaging session. PET/MRI also has the potential to significantly improve diagnostic workflows in neuro-oncology. Considering that a vast part of the population affected by brain tumors require both PET/CT and MRI during their clinical workup, a faster workflow would be considerably more convenient. The lower radiation exposure using MRI instead of CT is another important advantage. These aspects of the combined simultaneous approach are particularly relevant in patients with brain tumors, who generally need repeated scans. PET/MRI is particularly promising in the field of neuro-oncology, but large prospective trials are still needed to demonstrate its practical benefits to the scientific and clinical communities.

References

1. Siegel RL, Miller KD, Jemal A. Cancer statistics, 2016. CA Cancer J Clin. 2016;66(1):7–30.
2. Lin X, DeAngelis LM. Treatment of brain metastases. J Clin Oncol Off J Am Soc Clin Oncol. 2015;33(30):3475–84.
3. Louis DN, Ohgaki H, Wiestler OD, et al. The 2007 WHO classification of tumours of the central nervous system. Acta Neuropathol. 2007;114(2):97–109.
4. Louis DN, Perry A, Reifenberger G, et al. The 2016 World Health Organization classification of tumors of the central nervous system: a summary. Acta Neuropathol. 2016;131(6):803–20.
5. Mabray MC, Barajas RF Jr, Cha S. Modern brain tumor imaging. Brain Tumor Res Treat. 2015;3(1):8–23.
6. Cha S. Neuroimaging in neuro-oncology. Neurotherapeutics. 2009;6(3):465–77.
7. Wen PY, Macdonald DR, Reardon DA, et al. Updated response assessment criteria for high-grade gliomas: response assessment in neuro-oncology working group. J Clin Oncol Off J Am Soc Clin Oncol. 2010;28(11):1963–72.
8. Brandsma D, Stalpers L, Taal W, Sminia P, van den Bent MJ. Clinical features, mechanisms, and management of pseudoprogression in malignant gliomas. Lancet Oncol. 2008;9(5):453–61.
9. Gahramanov S, Muldoon LL, Varallyay CG, et al. Pseudoprogression of glioblastoma after chemo- and radiation therapy: diagnosis by using dynamic susceptibility-weighted contrast-enhanced perfusion MR imaging with ferumoxytol versus gadoteridol and correlation with survival. Radiology. 2013;266(3):842–52.
10. Weller M, van den Bent M, Hopkins K, et al. EANO guideline for the diagnosis and treatment of anaplastic gliomas and glioblastoma. Lancet Oncol. 2014;15(9):e395–403.
11. Fink JR, Muzi M, Peck M, Krohn KA. Multimodality brain tumor imaging: MR imaging, PET, and PET/MR imaging. J Nucl Med. 2015;56(10):1554–61.
12. Cha S. Update on brain tumor imaging. Curr Neurol Neurosci Rep. 2005;5(3):169–77.
13. Bruzzone MG, D'Incerti L, Farina LL, Cuccarini V, Finocchiaro G. CT and MRI of brain tumors. The quarterly journal of nuclear medicine and molecular imaging: official publication of the Italian Association of Nuclear Medicine (AIMN) [and] the International Association of Radiopharmacology (IAR), [and] Section of the Society of…. 2012;56(2):112–37.
14. Chourmouzi D, Papadopoulou E, Marias K, Drevelegas A. Imaging of brain tumors. Surg Oncol Clin N Am. 2014;23(4):629–84.

15. Kim M, Kim HS. Emerging techniques in brain tumor imaging: what radiologists need to know. Korean J Radiol. 2016;17(5):598–619.
16. Mohammadzadeh A, Mohammadzadeh V, Kooraki S, et al. Pretreatment evaluation of Glioma. Neuroimaging Clin N Am. 2016;26(4):567–80.
17. Upadhyay N, Waldman AD. Conventional MRI evaluation of gliomas. Br J Radiol. 2011;84(2):S107–11.
18. Grossman R, Shimony N, Shir D, et al. Dynamics of FLAIR volume changes in glioblastoma and prediction of survival. Ann Surg Oncol. 2016;24(3):794–800.
19. Wintersperger BJ, Runge VM, Biswas J, Reiser MF, Schoenberg SO. Brain tumor enhancement in MR imaging at 3 tesla: comparison of SNR and CNR gain using TSE and GRE techniques. Investig Radiol. 2007;42(8):558–63.
20. Yoo DH, Song SW, Yun TJ, et al. MR imaging evaluation of Intracerebral Hemorrhages and T2 Hyperintense white matter lesions appearing after radiation therapy in adult patients with primary brain tumors. PLoS One. 2015;10(8):e0136795.
21. Brandao LA, Shiroishi MS, Law M. Brain tumors: a multimodality approach with diffusion-weighted imaging, diffusion tensor imaging, magnetic resonance spectroscopy, dynamic susceptibility contrast and dynamic contrast-enhanced magnetic resonance imaging. Magn Reson Imaging Clin N Am. 2013;21(2):199–239.
22. Castellano A, Falini A. Progress in neuro-imaging of brain tumors. Curr Opin Oncol. 2016;28(6):484–93.
23. Baehring JM, Fulbright RK. Diffusion-weighted MRI in neuro-oncology. CNS Oncol. 2012;1(2):155–67.
24. Svolos P, Kousi E, Kapsalaki E, et al. The role of diffusion and perfusion weighted imaging in the differential diagnosis of cerebral tumors: a review and future perspectives. Cancer Imaging. 2014;14:20.
25. Pujol S, Wells W, Pierpaoli C, et al. The DTI challenge: toward standardized evaluation of diffusion tensor imaging tractography for neurosurgery. J Neuroimaging. 2015;25(6):875–82.
26. Ulmer JL, Klein AP, Mueller WM, DeYoe EA, Mark LP. Preoperative diffusion tensor imaging: improving neurosurgical outcomes in brain tumor patients. Neuroimaging Clin N Am. 2014;24(4):599–617.
27. Griffith B, Jain R. Perfusion imaging in neuro-oncology: basic techniques and clinical applications. Magn Reson Imaging Clin N Am. 2016;24(4):765–79.
28. Essig M, Shiroishi MS, Nguyen TB, et al. Perfusion MRI: the five most frequently asked technical questions. AJR Am J Roentgenol. 2013;200(1):24–34.
29. Grade M, Hernandez Tamames JA, Pizzini FB, Achten E, Golay X, Smits M. A neuroradiologist's guide to arterial spin labeling MRI in clinical practice. Neuroradiology. 2015;57(12):1181–202.
30. Noguchi T, Yoshiura T, Hiwatashi A, et al. Perfusion imaging of brain tumors using arterial spin-labeling: correlation with histopathologic vascular density. AJNR Am J Neuroradiol. 2008;29(4):688–93.
31. Kazda T, Bulik M, Pospisil P, et al. Advanced MRI increases the diagnostic accuracy of recurrent glioblastoma: single institution thresholds and validation of MR spectroscopy and diffusion weighted MR imaging. NeuroImage Clin. 2016;11:316–21.
32. Najac C, Ronen SMMR. Molecular imaging of brain cancer metabolism using hyperpolarized 13C magnetic resonance spectroscopy. Top Magn Reson Imaging. 2016;25(5):187–96.
33. Ross BD, Bhattacharya P, Wagner S, Tran T, Sailasuta N. Hyperpolarized MR imaging: neurologic applications of hyperpolarized metabolism. AJNR Am J Neuroradiol. 2010;31(1):24–33.
34. Bailey PD, Zaca D, Basha MM, et al. Presurgical fMRI and DTI for the prediction of perioperative motor and language deficits in primary or metastatic brain lesions. J Neuroimaging. 2015;25(5):776–84.
35. Voss J, Meier TB, Freidel R, et al. The role of secondary motor and language cortices in morbidity and mortality: a retrospective functional MRI study of surgical planning for patients with intracranial tumors. Neurosurg Focus. 2013;34(4):E7.

36. Colen RR, Hassan I, Elshafeey N, Zinn PO. Shedding light on the 2016 World Health Organization classification of tumors of the central nervous system in the era of radiomics and radiogenomics. Magn Reson Imaging Clin N Am. 2016;24(4):741–9.
37. ElBanan MG, Amer AM, Zinn PO, Colen RR. Imaging genomics of glioblastoma: state of the art bridge between genomics and neuroradiology. Neuroimaging Clin N Am. 2015;25(1):141–53.
38. Kotrotsou A, Zinn PO, Colen RR. Radiomics in brain Tumors: an emerging technique for characterization of tumor environment. Magn Reson Imaging Clin N Am. 2016;24(4):719–29.
39. Moton S, Elbanan M, Zinn PO, Colen RR. Imaging genomics of Glioblastoma: biology, biomarkers, and breakthroughs. Top Magn Reson Imaging. 2015;24(3):155–63.
40. Belliveau JG, Bauman G, Macdonald DR. Detecting tumor progression in glioma: current standards and new techniques. Expert Rev Anticancer Ther. 2016;16(11):1177–88.
41. Huang RY, Neagu MR, Reardon DA, Wen PY. Pitfalls in the neuroimaging of glioblastoma in the era of antiangiogenic and immuno/targeted therapy - detecting illusive disease, defining response. Front Neurol. 2015;6:33.
42. Syrota A, Comar D, Cerf M, Plummer D, Maziere M, Kellershohn C. [11C]methionine pancreatic scanning with positron emission computed tomography. J Nucl Med. 1979;20(7):778–81.
43. Ishiwata K, Kubota K, Murakami M, et al. Re-evaluation of amino acid PET studies: can the protein synthesis rates in brain and tumor tissues be measured in vivo? J Nucl Med. 1993;34(11):1936–43.
44. Wester HJ, Herz M, Weber W, et al. Synthesis and radiopharmacology of O-(2-[18F] fluoroethyl)-L-tyrosine for tumor imaging. J Nucl Med. 1999;40(1):205–12.
45. Weckesser M, Langen KJ, Rickert CH, et al. O-(2-[18F]fluorethyl)-L-tyrosine PET in the clinical evaluation of primary brain tumours. Eur J Nucl Med Mol Imaging. 2005;32(4):422–9.
46. Grosu AL, Astner ST, Riedel E, et al. An interindividual comparison of O-(2-[18F] fluoroethyl)-L-tyrosine (FET)- and L-[methyl-11C]methionine (MET)-PET in patients with brain gliomas and metastases. Int J Radiat Oncol Biol Phys. 2011;81(4):1049–58.
47. Becherer A, Karanikas G, Szabo M, et al. Brain tumour imaging with PET: a comparison between [18F]fluorodopa and [11C]methionine. Eur J Nucl Med Mol Imaging. 2003;30(11):1561–7.
48. Kratochwil C, Combs SE, Leotta K, et al. Intra-individual comparison of (1)(8)F-FET and (1)(8)F-DOPA in PET imaging of recurrent brain tumors. Neuro-Oncology. 2014;16(3):434–40.
49. Villani V, Carapella CM, Chiaravalloti A, et al. The role of PET [18F]FDOPA in evaluating low-grade glioma. Anticancer Res. 2015;35(9):5117–22.
50. Kondo A, Ishii H, Aoki S, et al. Phase IIa clinical study of [18F]fluciclovine: efficacy and safety of a new PET tracer for brain tumors. Ann Nucl Med. 2016;30(9):608–18.
51. Sasajima T, Ono T, Shimada N, et al. Trans-1-amino-3-18F-fluorocyclobutanecarboxylic acid (anti-18F-FACBC) is a feasible alternative to 11C-methyl-L-methionine and magnetic resonance imaging for monitoring treatment response in gliomas. Nucl Med Biol. 2013;40(6):808–15.
52. Albert NL, Weller M, Suchorska B, et al. Response assessment in neuro-oncology working group and European Association for Neuro-Oncology recommendations for the clinical use of PET imaging in gliomas. Neuro-Oncology. 2016;18(9):1199–208.
53. Pichler R, Dunzinger A, Wurm G, et al. Is there a place for FET PET in the initial evaluation of brain lesions with unknown significance? Eur J Nucl Med Mol Imaging. 2010;37(8):1521–8.
54. Bette S, Gempt J, Delbridge C, et al. Prognostic value of O-(2-[18F]-Fluoroethyl)-L-tyrosine-positron emission tomography imaging for histopathologic characteristics and progression-free survival in patients with low-grade glioma. World Neurosurg. 2016;89:230–9.
55. Dunet V, Rossier C, Buck A, Stupp R, Prior JO. Performance of 18F-fluoro-ethyl-tyrosine (18F-FET) PET for the differential diagnosis of primary brain tumor: a systematic review and metaanalysis. J Nucl Med. 2012;53(2):207–14.
56. Hutterer M, Nowosielski M, Putzer D, et al. [18F]-fluoro-ethyl-L-tyrosine PET: a valuable diagnostic tool in neuro-oncology, but not all that glitters is glioma. Neuro-Oncology. 2013;15(3):341–51.

57. Rapp M, Heinzel A, et al. Diagnostic performance of 18F-FET PET in newly diagnosed cerebral lesions suggestive of glioma. J Nucl Med. 2013;54(2):229–35
58. Jansen NL, Schwartz C, Graute V, et al. Prediction of oligodendroglial histology and LOH 1p/19q using dynamic [(18)F]FET-PET imaging in intracranial WHO grade II and III gliomas. Neuro-Oncology. 2012;14(12):1473–80.
59. Saito T, Maruyama T, Muragaki Y, et al. 11C-methionine uptake correlates with combined 1p and 19q loss of heterozygosity in oligodendroglial tumors. AJNR Am J Neuroradiol. 2013;34(1):85–91.
60. Pirotte BJ, Levivier M, Goldman S, et al. Positron emission tomography-guided volumetric resection of supratentorial high-grade gliomas: a survival analysis in 66 consecutive patients. Neurosurgery. 2009;64(3):471–81. discussion 81.
61. Popperl G, Kreth FW, Mehrkens JH, et al. FET PET for the evaluation of untreated gliomas: correlation of FET uptake and uptake kinetics with tumour grading. Eur J Nucl Med Mol Imaging. 2007;34(12):1933–42.
62. Kim S, Chung JK, Im SH, et al. 11C-methionine PET as a prognostic marker in patients with glioma: comparison with 18F-FDG PET. Eur J Nucl Med Mol Imaging. 2005;32(1): 52–9.
63. Van Laere K, Ceyssens S, Van Calenbergh F, et al. Direct comparison of 18F-FDG and 11C-methionine PET in suspected recurrence of glioma: sensitivity, inter-observer variability and prognostic value. Eur J Nucl Med Mol Imaging. 2005;32(1):39–51.
64. Floeth FW, Pauleit D, Sabel M, et al. Prognostic value of O-(2-18F-fluoroethyl)-L-tyrosine PET and MRI in low-grade glioma. J Nucl Med. 2007;48(4):519–27.
65. Morana G, Piccardo A, Puntoni M, et al. Diagnostic and prognostic value of 18F-DOPA PET and 1H-MR spectroscopy in pediatric supratentorial infiltrative gliomas: a comparative study. Neuro-Oncology. 2015;17(12):1637–47.
66. Popperl G, Kreth FW, Herms J, et al. Analysis of 18F-FET PET for grading of recurrent gliomas: is evaluation of uptake kinetics superior to standard methods? J Nucl Med. 2006;47(3):393–403.
67. Galldiks N, Stoffels G, Filss CP, et al. Role of O-(2-(18)F-fluoroethyl)-L-tyrosine PET for differentiation of local recurrent brain metastasis from radiation necrosis. J Nucl Med. 2012;53(9):1367–74.
68. Gonzalez-Forero M, Prieto E, Dominguez I, Vigil C, Penuelas I, Arbizu J. Dual time point 18F-FDOPA PET as a tool for characterizing brain tumors. Rev Esp Med Nucl. 2011;30(2):88–93.
69. Schiepers C, Chen W, Cloughesy T, Dahlbom M, Huang SC. 18F-FDOPA kinetics in brain tumors. J Nucl Med. 2007;48(10):1651–61.
70. Moulin-Romsee G, D'Hondt E, de Groot T, et al. Non-invasive grading of brain tumours using dynamic amino acid PET imaging: does it work for 11C-methionine? Eur J Nucl Med Mol Imaging. 2007;34(12):2082–7.
71. Grosu AL, Weber WA. PET for radiation treatment planning of brain tumours. Radiother Oncol. 2010;96(3):325–7.
72. Pafundi DH, Laack NN, Youland RS, et al. Biopsy validation of 18F-DOPA PET and biodistribution in gliomas for neurosurgical planning and radiotherapy target delineation: results of a prospective pilot study. Neuro-Oncology. 2013;15(8):1058–67.
73. Pauleit D, Floeth F, Hamacher K, et al. O-(2-[18F]fluoroethyl)-L-tyrosine PET combined with MRI improves the diagnostic assessment of cerebral gliomas. Brain. 2005;128(Pt 3):678–87.
74. Weber DC, Zilli T, et al. [(18)F]Fluoroethyltyrosine- positron emission tomography-guided radiotherapy for high-grade glioma. Radiat Oncol. 2008;3:44.
75. Nowosielski M, DiFranco MD, et al. An intra-individual comparison of MRI, [18F]-FET and [18F]-FLT PET in patients with high-grade gliomas. PLoS One. 2014;9(4):e95830.
76. Niyazi M, Geisler J, et al. FET-PET for malignant glioma treatment planning. Radiother Oncol. 2011;99(1):44–8.

77. Rosenschold P, Costa J, et al. Impact of [18F]-fluoro-ethyl-tyrosine PET imaging on target definition for radiation therapy of high-grade glioma. Neuro-Oncology. 2015;17(5):757–63.
78. Rieken S, Habermehl D, et al. Analysis of FET-PET imaging for target volume definition in patients with gliomas treated with conformal radiotherapy. Radiother Oncol. 2013;109(3):487–92.
79. Badakhshi H, Graf R, et al. The impact of 18 F-FET PET-CT on target definition in image-guided stereotactic radiotherapy in patients with skull base lesions. Cancer Imaging. 2014;14:25.
80. Piroth MD, Pinkawa M, Holy R, et al. Integrated boost IMRT with FET-PET-adapted local dose escalation in glioblastomas. Results of a prospective phase II study. Strahlenther Onkol. 2012;188(4):334–9.
81. Grosu AL, Weber WA, Riedel E, et al. L-(methyl-11C) methionine positron emission tomography for target delineation in resected high-grade gliomas before radiotherapy. Int J Radiat Oncol Biol Phys. 2005;63(1):64–74.
82. Oehlke O, Mix M, Graf E, et al. Amino-acid PET versus MRI guided re-irradiation in patients with recurrent glioblastoma multiforme (GLIAA) - protocol of a randomized phase II trial (NOA 10/ARO 2013-1). BMC Cancer. 2016;16(1):769.
83. Piroth MD, Holy R, Pinkawa M, et al. Prognostic impact of postoperative, pre-irradiation (18)F-fluoroethyl-l-tyrosine uptake in glioblastoma patients treated with radiochemotherapy. Radiother Oncol. 2011;99(2):218–24.
84. Galldiks N, Dunkl V, Stoffels G, et al. Diagnosis of pseudoprogression in patients with glioblastoma using O-(2-[18F]fluoroethyl)-L-tyrosine PET. Eur J Nucl Med Mol Imaging. 2015;42(5):685–95.
85. Galldiks N, Rapp M, Stoffels G, Dunkl V, Sabel M, Langen KJ. Earlier diagnosis of progressive disease during bevacizumab treatment using O-(2-18F-fluorethyl)-L-tyrosine positron emission tomography in comparison with magnetic resonance imaging. Mol Imaging. 2013;12(5):273–6.
86. Heinzel A, Muller D, Langen KJ, et al. The use of O-(2-18F-fluoroethyl)-L-tyrosine PET for treatment management of bevacizumab and irinotecan in patients with recurrent high-grade glioma: a cost-effectiveness analysis. J Nucl Med. 2013;54(8):1217–22.
87. Galldiks N, Stoffels G, et al. Role of O-(2-(18)F-fluoroethyl)-L-tyrosine PET for differentiation of local recurrent brain metastasis from radiation necrosis. J Nucl Med. 2012;53(9):1367–74.
88. Galldiks N, Stoffels G, et al. Role of O-(2-18F-fluoroethyl)-L-tyrosine PET as a diagnostic tool for detection of malignant progression in patients with low-grade glioma. J Nucl Med. 2013;54(12):2046–54.
89. Momose T, Nariai T, Kawabe T, et al. Clinical benefit of 11C methionine PET imaging as a planning modality for radiosurgery of previously irradiated recurrent brain metastases. Clin Nucl Med. 2014;39(11):939–43.
90. Pirotte BJ, Lubansu A, Massager N, et al. Clinical impact of integrating positron emission tomography during surgery in 85 children with brain tumors. J Neurosurg Pediatr. 2010;5(5):486–99.
91. Romagna A, Unterrainer M, Schmid-Tannwald C, et al. Suspected recurrence of brain metastases after focused high dose radiotherapy: can [18F]FET- PET overcome diagnostic uncertainties? Radiat Oncol. 2016;11(1):139.
92. Terakawa Y, Tsuyuguchi N, Iwai Y, et al. Diagnostic accuracy of 11C-methionine PET for differentiation of recurrent brain tumors from radiation necrosis after radiotherapy. J Nucl Med. 2008;49(5):694–9.
93. Herrmann K, Czernin J, Cloughesy T, et al. Comparison of visual and semiquantitative analysis of 18F-FDOPA-PET/CT for recurrence detection in glioblastoma patients. Neuro-Oncology. 2014;16(4):603–9.
94. Minamimoto R, Saginoya T, Kondo C, et al. Differentiation of brain tumor recurrence from post-radiotherapy necrosis with 11C-methionine PET: visual assessment versus quantitative assessment. PLoS One. 2015;10(7):e0132515.

95. Spence AM, Muzi M, Mankoff DA, et al. 18F-FDG PET of gliomas at delayed intervals: improved distinction between tumor and normal gray matter. J Nucl Med. 2004;45(10):1653–9.
96. Prieto E, Marti-Climent JM, Dominguez-Prado I, et al. Voxel-based analysis of dual-time-point 18F-FDG PET images for brain tumor identification and delineation. J Nucl Med. 2011;52(6):865–72.
97. Roelcke U, Blasberg RG, von Ammon K, et al. Dexamethasone treatment and plasma glucose levels: relevance for fluorine-18-fluorodeoxyglucose uptake measurements in gliomas. J Nucl Med. 1998;39(5):879–84.
98. Lewitschnig S, Gedela K, Toby M, et al. (1)(8)F-FDG PET/CT in HIV-related central nervous system pathology. Eur J Nucl Med Mol Imaging. 2013;40(9):1420–7.
99. Alavi JB, Alavi A, Chawluk J, et al. Positron emission tomography in patients with glioma. A predictor of prognosis. Cancer. 1988;62(6):1074–8.
100. Colavolpe C, Chinot O, Metellus P, et al. FDG-PET predicts survival in recurrent high-grade gliomas treated with bevacizumab and irinotecan. Neuro-Oncology. 2012;14(5):649–57.
101. Padma MV, Said S, Jacobs M, et al. Prediction of pathology and survival by FDG PET in gliomas. J Neuro-Oncol. 2003;64(3):227–37.
102. Delbeke D, Meyerowitz C, Lapidus RL, et al. Optimal cutoff levels of F-18 fluorodeoxyglucose uptake in the differentiation of low-grade from high-grade brain tumors with PET. Radiology. 1995;195(1):47–52.
103. Jacobs AH, Kracht LW, Gossmann A, et al. Imaging in neurooncology. NeuroRx. 2005;2(2):333–47.
104. Kasenda B, Haug V, Schorb E, et al. 18F-FDG PET is an independent outcome predictor in primary central nervous system lymphoma. J Nucl Med. 2013;54(2):184–91.
105. Hillner BE, Siegel BA, et al. Impact of dedicated brain PET on intended patient management in participants of the national oncologic PET Registry. Mol Imaging Biol. 2011;13(1):161–5.
106. Herholz K, Langen KJ, Schiepers C, Mountz JM. Brain tumors. Semin Nucl Med. 2012;42(6):356–70.
107. Caroline I, Rosenthal MA. Imaging modalities in high-grade gliomas: pseudoprogression, recurrence, or necrosis? J Clin Neurosci. 2012;19(5):633–7.
108. Mottram JC. Factors of importance in the radiosensitivity of tumors. Br J Radiol. 1936;9:606–14.
109. Padhani AR, Krohn KA, Lewis JS, Alber M. Imaging oxygenation of human tumours. Eur Radiol. 2007;17(4):861–72.
110. Vaupel P. The role of hypoxia-induced factors in tumor progression. Oncologist. 2004;9(Suppl 5):10–7.
111. Mendichovszky I, Jackson A. Imaging hypoxia in gliomas. Br J Radiol. 2011;84(2):S145–58.
112. Bruehlmeier M, Roelcke U, Schubiger PA, Ametamey SM. Assessment of hypoxia and perfusion in human brain tumors using PET with 18F-fluoromisonidazole and 15O-H2O. J Nucl Med. 2004;45(11):1851–9.
113. Gulyas B, Halldin C. New PET radiopharmaceuticals beyond FDG for brain tumor imaging. The quarterly journal of nuclear medicine and molecular imaging : official publication of the Italian Association of Nuclear Medicine (AIMN) [and] the International Association of Radiopharmacology (IAR), [and] Section of the Society of…. 2012;56(2):173–90.
114. Bell C, Dowson N, Fay M, et al. Hypoxia imaging in gliomas with 18F-fluoromisonidazole PET: toward clinical translation. Semin Nucl Med. 2015;45(2):136–50.
115. Valk PE, Mathis CA, Prados MD, Gilbert JC, Budinger TF. Hypoxia in human gliomas: demonstration by PET with fluorine-18-fluoromisonidazole. J Nucl Med. 1992;33(12):2133–7.
116. Spence AM, Muzi M, Swanson KR, et al. Regional hypoxia in glioblastoma multiforme quantified with [18F]fluoromisonidazole positron emission tomography before radiotherapy: correlation with time to progression and survival. Clin Cancer Res. 2008;14(9):2623–30.
117. Hirata K, Terasaka S, Shiga T, et al. (1)(8)F-Fluoromisonidazole positron emission tomography may differentiate glioblastoma multiforme from less malignant gliomas. Eur J Nucl Med Mol Imaging. 2012;39(5):760–70.

118. Yamamoto Y, Maeda Y, Kawai N, et al. Hypoxia assessed by 18F-fluoromisonidazole positron emission tomography in newly diagnosed gliomas. Nucl Med Commun. 2012;33(6):621–5.
119. De Clermont H, Huchet A, Lamare F, Riviere A, Fernandez P. Lack of concordance between the F-18 fluoromisonidazole PET and the F-18 FDG PET in human glioblastoma. Clin Nucl Med. 2011;36(12):e194–5.
120. Rajendran JG, Mankoff DA, O'Sullivan F, et al. Hypoxia and glucose metabolism in malignant tumors: evaluation by [18F]fluoromisonidazole and [18F]fluorodeoxyglucose positron emission tomography imaging. Clin Cancer Res. 2004;10(7):2245–52.
121. Toyonaga T, Hirata K, Yamaguchi S, et al. (18)F-fluoromisonidazole positron emission tomography can predict pathological necrosis of brain tumors. Eur J Nucl Med Mol Imaging. 2016;43(8):1469–76.
122. Gerstner ER, Zhang Z, Fink JR, et al. ACRIN 6684: assessment of tumor hypoxia in newly diagnosed Glioblastoma using 18F-FMISO PET and MRI. Clin Cancer Res. 2016;22(20):5079–86.
123. Dewhirst MW, Cao Y, Moeller B. Cycling hypoxia and free radicals regulate angiogenesis and radiotherapy response. Nat Rev Cancer. 2008;8(6):425–37.
124. Thompson G, Mills SJ, Coope DJ, O'Connor JP, Jackson A. Imaging biomarkers of angiogenesis and the microvascular environment in cerebral tumours. Br J Radiol. 2011;84(2):S127–44.
125. Batchelor TT, Reardon DA, de Groot JF, Wick W, Weller M. Antiangiogenic therapy for glioblastoma: current status and future prospects. Clin Cancer Res. 2014;20(22):5612–9.
126. Iagaru A, Chen X, Gambhir SS. Molecular imaging can accelerate anti-angiogenic drug development and testing. Nat Clin Pract Oncol. 2007;4(10):556–7.
127. Iagaru A, Gambhir SS. Imaging tumor angiogenesis: the road to clinical utility. AJR Am J Roentgenol. 2013;201(2):W183–91.
128. Minamimoto R, Jamali M, Barkhodari A, et al. Biodistribution of the (1)(8)F-FPPRGD(2) PET radiopharmaceutical in cancer patients: an atlas of SUV measurements. Eur J Nucl Med Mol Imaging. 2015;42(12):1850–8.
129. Treglia G, Giovannini E, Di Franco D, et al. The role of positron emission tomography using carbon-11 and fluorine-18 choline in tumors other than prostate cancer: a systematic review. Ann Nucl Med. 2012;26(6):451–61.
130. DeGrado TR, Baldwin SW, Wang S, et al. Synthesis and evaluation of (18)F-labeled choline analogs as oncologic PET tracers. J Nucl Med. 2001;42(12):1805–14.
131. Hara T, Kosaka N, Shinoura N, Kondo T. PET imaging of brain tumor with [methyl-11C] choline. J Nucl Med. 1997;38(6):842–7.
132. Hara T, Kondo T, Hara T, Kosaka N. Use of 18F-choline and 11C-choline as contrast agents in positron emission tomography imaging-guided stereotactic biopsy sampling of gliomas. J Neurosurg. 2003;99(3):474–9.
133. Ohtani T, Kurihara H, Ishiuchi S, et al. Brain tumour imaging with carbon-11 choline: comparison with FDG PET and gadolinium-enhanced MR imaging. Eur J Nucl Med. 2001;28(11):1664–70.
134. Utriainen M, Komu M, Vuorinen V, et al. Evaluation of brain tumor metabolism with [11C] choline PET and 1H-MRS. J Neuro-Oncol. 2003;62(3):329–38.
135. Tian M, Zhang H, Higuchi T, Oriuchi N, Endo K. Oncological diagnosis using (11)C-choline-positron emission tomography in comparison with 2-deoxy-2-[(18)F] fluoro-D-glucose-positron emission tomography. Mol Imaging Biol. 2004;6(3):172–9.
136. Tian M, Zhang H, Oriuchi N, Higuchi T, Endo K. Comparison of 11C-choline PET and FDG PET for the differential diagnosis of malignant tumors. Eur J Nucl Med Mol Imaging. 2004;31(8):1064–72.
137. Kwee SA, Ko JP, Jiang CS, Watters MR, Coel MN. Solitary brain lesions enhancing at MR imaging: evaluation with fluorine 18 fluorocholine PET. Radiology. 2007;244(2):557–65.
138. Huang Z, Zuo C, Guan Y, et al. Misdiagnoses of 11C-choline combined with 18F-FDG PET imaging in brain tumours. Nucl Med Commun. 2008;29(4):354–8.

139. Kato T, Shinoda J, Nakayama N, et al. Metabolic assessment of gliomas using 11C-methionine, [18F] fluorodeoxyglucose, and 11C-choline positron-emission tomography. AJNR Am J Neuroradiol. 2008;29(6):1176–82.
140. Takenaka S, Shinoda J, Asano Y, et al. Metabolic assessment of monofocal acute inflammatory demyelination using MR spectroscopy and (11)C-methionine-, (11)C-choline-, and (18) F-fluorodeoxyglucose-PET. Brain Tumor Pathol. 2011;28(3):229–38.
141. Tan H, Chen L, Guan Y, Lin X. Comparison of MRI, F-18 FDG, and 11C-choline PET/CT for their potentials in differentiating brain tumor recurrence from brain tumor necrosis following radiotherapy. Clin Nucl Med. 2011;36(11):978–81.
142. Li FM, Nie Q, Wang RM, et al. 11C-CHO PET in optimization of target volume delineation and treatment regimens in postoperative radiotherapy for brain gliomas. Nucl Med Biol. 2012;39(3):437–42.
143. Gomez-Rio M, Testart Dardel N, Santiago Chinchilla A, et al. (1)(8)F-Fluorocholine PET/CT as a complementary tool in the follow-up of low-grade glioma: diagnostic accuracy and clinical utility. Eur J Nucl Med Mol Imaging. 2015;42(6):886–95.
144. Giovacchini G, Fallanca F, Landoni C, et al. C-11 choline versus F-18 fluorodeoxyglucose for imaging meningiomas: an initial experience. Clin Nucl Med. 2009;34(1):7–10.
145. Vander Borght T, Labar D, Pauwels S, Lambotte L. Production of [2-11C]thymidine for quantification of cellular proliferation with PET. Int J Radiat Appl Instrum Part A. 1991;42(1):103–4.
146. Shields AF, Grierson JR, Dohmen BM, et al. Imaging proliferation in vivo with [F-18]FLT and positron emission tomography. Nat Med. 1998;4(11):1334–6.
147. Shinomiya A, Kawai N, Okada M, et al. Evaluation of 3′-deoxy-3′-[18F]-fluorothymidine (18F-FLT) kinetics correlated with thymidine kinase-1 expression and cell proliferation in newly diagnosed gliomas. Eur J Nucl Med Mol Imaging. 2013;40(2):175–85.
148. Tripathi M, Sharma R, D'Souza M, et al. Comparative evaluation of F-18 FDOPA, F-18 FDG, and F-18 FLT-PET/CT for metabolic imaging of low grade gliomas. Clin Nucl Med. 2009;34(12):878–83.
149. Collet S, Valable S, Constans JM, et al. [(18)F]-fluoro-L-thymidine PET and advanced MRI for preoperative grading of gliomas. NeuroImage Clin. 2015;8:448–54.
150. Yamamoto Y, Ono Y, Aga F, Kawai N, Kudomi N, Nishiyama Y. Correlation of 18F-FLT uptake with tumor grade and Ki-67 immunohistochemistry in patients with newly diagnosed and recurrent gliomas. J Nucl Med. 2012;53(12):1911–5.
151. Choi SJ, Kim JS, Kim JH, et al. [18F]3′-deoxy-3′-fluorothymidine PET for the diagnosis and grading of brain tumors. Eur J Nucl Med Mol Imaging. 2005;32(6):653–9.
152. Ferdova E, Ferda J, Baxa J, et al. Assessment of grading in newly-diagnosed glioma using 18F-fluorothymidine PET/CT. Anticancer Res. 2015;35(2):955–9.
153. Chen W, Cloughesy T, Kamdar N, et al. Imaging proliferation in brain tumors with 18F-FLT PET: comparison with 18F-FDG. J Nucl Med. 2005;46(6):945–52.
154. Jacobs AH, Thomas A, Kracht LW, et al. 18F-fluoro-L-thymidine and 11C-methylmethionine as markers of increased transport and proliferation in brain tumors. J Nucl Med. 2005;46(12):1948–58.
155. Li Z, Yu Y, Zhang H, Xu G, Chen L. A meta-analysis comparing 18F-FLT PET with 18F-FDG PET for assessment of brain tumor recurrence. Nucl Med Commun. 2015;36(7):695–701.
156. Hatakeyama T, Kawai N, Nishiyama Y, et al. 11C-methionine (MET) and 18F-fluorothymidine (FLT) PET in patients with newly diagnosed glioma. Eur J Nucl Med Mol Imaging. 2008;35(11):2009–17.
157. Enslow MS, Zollinger LV, Morton KA, et al. Comparison of 18F-fluorodeoxyglucose and 18F-fluorothymidine PET in differentiating radiation necrosis from recurrent glioma. Clin Nucl Med. 2012;37(9):854–61.
158. Shishido H, Kawai N, Miyake K, Yamamoto Y, Nishiyama Y, Tamiya T. Diagnostic value of 11C-methionine (MET) and 18F-Fluorothymidine (FLT) positron emission tomography in recurrent high-grade Gliomas; differentiation from treatment-induced tissue necrosis. Cancers. 2012;4(1):244–56.

159. Chen W, Delaloye S, Silverman DH, et al. Predicting treatment response of malignant gliomas to bevacizumab and irinotecan by imaging proliferation with [18F] fluorothymidine positron emission tomography: a pilot study. J Clin Oncol Off J Am Soc Clin Oncol. 2007;25(30):4714–21.
160. Harris RJ, Cloughesy TF, Pope WB, et al. 18F-FDOPA and 18F-FLT positron emission tomography parametric response maps predict response in recurrent malignant gliomas treated with bevacizumab. Neuro-Oncology. 2012;14(8):1079–89.
161. Schwarzenberg J, Czernin J, Cloughesy TF, et al. 3′-deoxy-3′-18F-fluorothymidine PET and MRI for early survival predictions in patients with recurrent malignant glioma treated with bevacizumab. J Nucl Med. 2012;53(1):29–36.
162. Wardak M, Schiepers C, Cloughesy TF, Dahlbom M, Phelps ME, Huang SC. (1)(8)F-FLT and (1)(8)F-FDOPA PET kinetics in recurrent brain tumors. Eur J Nucl Med Mol Imaging. 2014;41(6):1199–209.
163. Wardak M, Schiepers C, Dahlbom M, et al. Discriminant analysis of (1)(8)F-fluorothymidine kinetic parameters to predict survival in patients with recurrent high-grade glioma. Clin Cancer Res. 2011;17(20):6553–62.
164. Ma DJ, Galanis E, Anderson SK, et al. A phase II trial of everolimus, temozolomide, and radiotherapy in patients with newly diagnosed glioblastoma: NCCTG N057K. Neuro-Oncology. 2015;17(9):1261–9.
165. Leung K. [11C]acetate. Molecular imaging and contrast agent database (MICAD). Bethesda: National Center for Biotechnology Information (US); 2004.
166. Pike VW, Eakins MN, Allan RM, Selwyn AP. Preparation of [1-11C]acetate--an agent for the study of myocardial metabolism by positron emission tomography. Int J Appl Radiat Isot. 1982;33(7):505–12.
167. Liu RS, Chang CP, Chu LS, et al. PET imaging of brain astrocytoma with 1-11C-acetate. Eur J Nucl Med Mol Imaging. 2006;33(4):420–7.
168. Liu RS, Chang CP, Guo WY, et al. 1-11C-acetate versus 18F-FDG PET in detection of meningioma and monitoring the effect of gamma-knife radiosurgery. J Nucl Med. 2010;51(6):883–91.
169. Tsuchida T, Takeuchi H, Okazawa H, Tsujikawa T, Fujibayashi Y. Grading of brain glioma with 1-11C-acetate PET: comparison with 18F-FDG PET. Nucl Med Biol. 2008;35(2):171–6.
170. Yamamoto Y, Nishiyama Y, Kimura N, et al. 11C-acetate PET in the evaluation of brain glioma: comparison with 11C-methionine and 18F-FDG-PET. Mol Imaging Biol. 2008;10(5):281–7.
171. Al-Nahhas A, Win Z, Szyszko T, et al. Gallium-68 PET: a new frontier in receptor cancer imaging. Anticancer Res. 2007;27(6b):4087–94.
172. Silva CB, Ongaratti BR, Trott G, et al. Expression of somatostatin receptors (SSTR1-SSTR5) in meningiomas and its clinicopathological significance. Int J Clin Exp Pathol. 2015;8(10):13185–92.
173. Combs SE, Welzel T, Habermehl D, et al. Prospective evaluation of early treatment outcome in patients with meningiomas treated with particle therapy based on target volume definition with MRI and 68Ga-DOTATOC-PET. Acta Oncol (Stockh.). 2013;52(3):514–20.
174. Gehler B, Paulsen F, Oksuz MO, et al. [68Ga]-DOTATOC-PET/CT for meningioma IMRT treatment planning. Radiat Oncol. 2009;4:56.
175. Graf R, Nyuyki F, Steffen IG, et al. Contribution of 68Ga-DOTATOC PET/CT to target volume delineation of skull base meningiomas treated with stereotactic radiation therapy. Int J Radiat Oncol Biol Phys. 2013;85(1):68–73.
176. Madani I, Lomax AJ, Albertini F, Trnkova P, Weber DC. Dose-painting intensity-modulated proton therapy for intermediate- and high-risk meningioma. Radiat Oncol. 2015;10:72.
177. Milker-Zabel S, Zabel-du Bois A, Henze M, et al. Improved target volume definition for fractionated stereotactic radiotherapy in patients with intracranial meningiomas by correlation of CT, MRI, and [68Ga]-DOTATOC-PET. Int J Radiat Oncol Biol Phys. 2006;65(1):222–7.
178. Nyuyki F, Plotkin M, Graf R, et al. Potential impact of (68)Ga-DOTATOC PET/CT on stereotactic radiotherapy planning of meningiomas. Eur J Nucl Med Mol Imaging. 2010;37(2):310–8.

179. Thorwarth D, Henke G, Muller AC, et al. Simultaneous 68Ga-DOTATOC-PET/MRI for IMRT treatment planning for meningioma: first experience. Int J Radiat Oncol Biol Phys. 2011;81(1):277–83.
180. Sommerauer M, Burkhardt JK, Frontzek K, et al. 68Gallium-DOTATATE PET in meningioma: a reliable predictor of tumor growth rate? Neuro-Oncology. 2016;18(7):1021–7.
181. Afshar-Oromieh A, Giesel FL, Linhart HG, et al. Detection of cranial meningiomas: comparison of (6)(8)Ga-DOTATOC PET/CT and contrast-enhanced MRI. Eur J Nucl Med Mol Imaging. 2012;39(9):1409–15.
182. Bodei L, Cremonesi M, Kidd M, et al. Peptide receptor radionuclide therapy for advanced neuroendocrine tumors. Thorac Surg Clin. 2014;24(3):333–49.
183. Hanscheid H, Sweeney RA, Flentje M, et al. PET SUV correlates with radionuclide uptake in peptide receptor therapy in meningioma. Eur J Nucl Med Mol Imaging. 2012;39(8):1284–8.
184. Seystahl K, Stoecklein V, Schuller U, et al. Somatostatin receptor-targeted radionuclide therapy for progressive meningioma: benefit linked to 68Ga-DOTATATE/−TOC uptake. Neuro-Oncology. 2016;18(11):1538–47.
185. Shao Y, Cherry SR, Farahani K, et al. Simultaneous PET and MR imaging. Phys Med Biol. 1997;42(10):1965–70.
186. Schlemmer HP, Pichler BJ, Schmand M, et al. Simultaneous MR/PET imaging of the human brain: feasibility study. Radiology. 2008;248(3):1028–35.
187. Delso G, Furst S, Jakoby B, et al. Performance measurements of the Siemens mMR integrated whole-body PET/MR scanner. J Nucl Med. 2011;52(12):1914–22.
188. Bisdas S, Ritz R, Bender B, et al. Metabolic mapping of gliomas using hybrid MR-PET imaging: feasibility of the method and spatial distribution of metabolic changes. Investig Radiol. 2013;48(5):295–301.
189. Boss A, Kolb A, Hofmann M, et al. Diffusion tensor imaging in a human PET/MR hybrid system. Investig Radiol. 2010;45(5):270–4.
190. Garibotto V, Heinzer S, Vulliemoz S, et al. Clinical applications of hybrid PET/MRI in neuroimaging. Clin Nucl Med. 2013;38(1):e13–8.
191. Neuner I, Kaffanke JB, Langen KJ, et al. Multimodal imaging utilising integrated MR-PET for human brain tumour assessment. Eur Radiol. 2012;22(12):2568–80.
192. Afshar-Oromieh A, Wolf MB, Kratochwil C, et al. Comparison of (6)(8)Ga-DOTATOC-PET/CT and PET/MRI hybrid systems in patients with cranial meningioma: initial results. Neuro-Oncology. 2015;17(2):312–9.
193. Jena A, Taneja S, Gambhir A, et al. Glioma recurrence versus radiation necrosis: single-session multiparametric approach using simultaneous O-(2-18F-Fluoroethyl)-L-tyrosine PET/MRI. Clin Nucl Med. 2016;41(5):e228–36.
194. Sacconi B, Raad RA, Lee J, et al. Concurrent functional and metabolic assessment of brain tumors using hybrid PET/MR imaging. J Neuro-Oncol. 2016;127(2):287–93.
195. Fraioli F, Shankar A, Hargrave D, et al. 18F-fluoroethylcholine (18F-Cho) PET/MRI functional parameters in pediatric astrocytic brain tumors. Clin Nucl Med. 2015;40(1):e40–5.
196. Preuss M, Werner P, Barthel H, et al. Integrated PET/MRI for planning navigated biopsies in pediatric brain tumors. Childs Nerv Syst. 2014;30(8):1399–403.
197. Boss A, Bisdas S, Kolb A, et al. Hybrid PET/MRI of intracranial masses: initial experiences and comparison to PET/CT. J Nucl Med. 2010;51(8):1198–205.
198. Schwenzer NF, Stegger L, Bisdas S, et al. Simultaneous PET/MR imaging in a human brain PET/MR system in 50 patients--current state of image quality. Eur J Radiol. 2012;81(11):3472–8.
199. Navarria P, Reggiori G, Pessina F, et al. Investigation on the role of integrated PET/MRI for target volume definition and radiotherapy planning in patients with high grade glioma. Radiother Oncol. 2014;112(3):425–9.
200. Filss CP, Galldiks N, Stoffels G, et al. Comparison of 18F-FET PET and perfusion-weighted MR imaging: a PET/MR imaging hybrid study in patients with brain tumors. J Nuclear Med. 2014;55(4):540–5.